

Fission Barriers Deduced from the Analysis of Fission Isomer Results*

H. C. Britt, M. Bolsterli, J. R. Nix, and J. L. Norton

Los Alamos Scientific Laboratory, University of California, Los Alamos, New Mexico 87544

(Received 1 November 1972)

Available experimental data on fission-isomer excitation functions have been reanalyzed using an improved statistical model to determine values for the energies relative to the ground state of the secondary minimum and second maximum in the fission barrier for a series of plutonium, americium, and curium isotopes. The statistical model incorporates realistic decay-width calculations for neutron emission, fission, and γ -ray emission which are based on nuclear level densities derived from appropriate single-particle-level spectra. Values for the curvature $\hbar\omega_B$ of the second barrier are also estimated from the observed fission-isomer half-lives. The fission-barrier shapes determined from the analysis of experimental results are compared to theoretical calculations of barriers performed by several groups. The experimental barrier parameters agree with a variety of theoretical calculations to an accuracy of about 1 MeV. Systematic deviations between the experimental and theoretical results suggest that the surface asymmetry constant κ in the liquid-drop mass formula should be substantially larger than the value of 1.7826 used in the second mass formula of Myers and Swiatecki.

I. INTRODUCTION

Information about the fission barriers of actinide nuclei can be obtained from the analysis of experimental data on fission isomers. In a recent paper¹ a statistical model was developed and used to fit excitation functions for the production of fission isomers in a variety of nuclei. The major deficiency in the formulation of this model was the calculation of the various decay widths by use of an empirical nuclear-level-density function² which was generalized to account for its deformation dependence in a rather arbitrary manner. In addition, the empirical level-density function does not correctly take into account the effects of nuclear shells on the energy dependence of the compound-nuclear level density. Recently it has been pointed out by several authors³⁻⁵ that it is possible to generate the dependence of the compound-nuclear level density on excitation energy directly from the spectrum of single-particle levels without resorting to empirical models. This approach automatically accounts for the effects of nuclear shells and in addition it is possible to take into account the effects of nuclear pairing in a natural way.⁶ The problem of obtaining variable level densities (and, thereby, decay widths) now becomes a problem of obtaining realistic single-particle spectra for cases of interest. This approach ties the statistical-model calculations to other areas of nuclear-structure physics and allows the direct input of information from other experimental and/or theoretical areas of nuclear physics.

In the actinide nuclei the existence of a two-peaked fission barrier is a result⁷ of the varia-

tion with deformation in the spacing of single-particle levels near the Fermi surface which leads to a correlated variation in the shell correction to the nuclear potential-energy surface. Since the variation of these shell effects with deformation is crucial in determining the shape of the potential-energy surfaces involved in the fission process it should also be anticipated that shell effects in the compound-nuclear level densities might be very important in any quantitative analysis of the dynamics of fission processes. In the calculation of fission-isomer excitation functions it is now possible to develop a nearly self-consistent statistical model by calculating neutron, γ -ray, and fission decay widths using compound level densities that are obtained from the theoretical single-particle level spectra generated in the potential energy calculations. In this model separate single-particle spectra at the relevant deformations (first minimum, first maximum, second minimum, and second maximum) can be used and to the extent that the parameters of the fission barrier deduced from fitting experimental data agree with the theoretical potential-energy calculations, this approach can yield a nearly self-consistent test of the theoretical calculations. This general approach is followed in the results presented below.

In the current statistical model we use single-particle level densities obtained from the theoretical model developed recently⁸ to calculate fission barriers for heavy nuclei. In the results presented in this paper currently available data on fission-isomer excitation functions^{1, 9-17} are analyzed to try to obtain energies relative to the ground state for the second minimum and second maximum of

the fission barrier. The calculations and the statistical model are checked by comparing to available data¹⁸⁻²³ on the excitation functions from production of nuclei in their ground states (i.e. spallation cross sections). Experimental results on fission-isomer half-lives^{1, 10, 11, 14, 15, 24-26} and spontaneous fission half-lives for decay from the ground state²⁷⁻³¹ are then used to estimate the curvatures ($\hbar\omega_B$ and $\hbar\omega_A$) of the two peaks in the fission barriers for many nuclei. For convenience the sources of the experimental data used in this paper are listed in Tables I-IV. The notation used to describe various aspects of the fission barrier is illustrated in Fig. 1.

TABLE I. Sources for the experimental data used in the determination of fission barrier parameters. Sources for fission-isomer-excitation-function data.

Isomer	Reaction	Source	Reference
²³⁵ Pu	²³³ U(α , 2n)	Britt <i>et al.</i>	1
²³⁷ Pu	²³⁵ U(α , 2n)	Britt <i>et al.</i>	1
	²³⁷ Np(d , 2n)	Britt <i>et al.</i>	1
	²³⁶ U(α , 3n)	Wolf and Unik	9
²³⁸ Pu	²³⁶ U(α , 2n)	Sletten and Limkilde	10
²³⁹ Pu	²³⁸ U(α , 3n)	Britt <i>et al.</i>	1
	²³⁸ U(α , 3n)	Wolf and Unik	9
²⁴⁰ Pu	²³⁸ U(α , 2n)	Britt <i>et al.</i>	1
²³⁷ Am	²³⁸ Pu(p , 2n)	Polikanov and Sletten	11
²³⁸ Am	²³⁹ Pu(p , 2n)	Sletten	12
	²³⁹ Pu(p , 2n)	Britt, Erkkila, and Back	13
²³⁹ Am	²³⁹ Pu(d , 2n)	Britt <i>et al.</i>	1
	²⁴⁰ Pu(p , 2n)	Lark <i>et al.</i>	14
	²⁴⁰ Pu(α , 3n)	Britt, Erkkila, and Back	13
	²³⁷ Np(α , 2n)	Britt <i>et al.</i>	1
²⁴⁰ Am	²⁴¹ Pu(p , 2n)	Björnholm <i>et al.</i>	15
	²⁴⁰ Pu(d , 2n)	Britt <i>et al.</i>	1
	²⁴⁰ Pu(t , 3n)	Britt, Erkkila, and Back	13
²⁴¹ Am	²⁴² Pu(p , 2n)	Britt, Erkkila, and Back	13
	²⁴² Pu(p , 2n)	Lark <i>et al.</i>	14
²⁴² Am	²⁴² Pu(d , 2n)	Britt <i>et al.</i>	1
	²⁴³ Am(n , 2n)	Flerov <i>et al.</i>	16
	²⁴² Pu(t , 3n)	Britt, Erkkila, and Back	13
²⁴³ Am	²⁴⁴ Pu(p , 2n)	Britt, Erkkila, and Back	13
²⁴⁴ Am	²⁴⁴ Pu(d , 2n)	Britt <i>et al.</i>	1
	²⁴⁴ Pu(t , 3n)	Britt, Erkkila, and Back	13
²⁴¹ Cm	²³⁹ Pu(α , 2n)	Britt <i>et al.</i>	1
²⁴³ Cm	²⁴² Pu(α , 3n)	Britt <i>et al.</i>	1
	²⁴² Pu(α , 3n)	Wolf and Unik	17
²⁴⁵ Cm	²⁴⁴ Pu(α , 3n)	Britt <i>et al.</i>	1
	²⁴⁴ Pu(α , 3n)	Wolf and Unik	17

II. STATISTICAL MODEL FOR ISOMER EXCITATION FUNCTIONS

A. General Characteristics

Except for the use of more realistic level densities in the calculation of the relevant decay widths (see Sec. II B below) the current statistical model is very similar to that used in the previous paper.¹ However, in several areas small improvements were made in the model by eliminating several unnecessary approximations. A schematic description of the statistical model as used in the present calculations is given in Secs. II A 1-II A 3 below. The calculations are schematically illustrated in Fig. 2. In the notation used A denotes the nucleus containing the observed fission isomer, $A + 1$ the nucleus which feeds the isomeric state by neutron evaporation, and $A + 2$ or $A + 3$ the compound nuclei formed in the original capture reaction. Comparisons to spallation data involve decay of the population in the first well for the A nucleus to the $A - 1$ nucleus.

1. Population of $A + 1$ Nucleus

The majority of the decays to the $A + 1$ nucleus populate states in the first potential well and for purposes of calculating the population of isomers in the A nucleus the small fraction ($\sim 10^{-4}$) of nuclei decaying directly from the second well can be ignored.

At the initial excitation energies involved in $3n$ reactions the fraction of the nuclei which undergo fission [$P_f = \Gamma_f / (\Gamma_f + \Gamma_n)$] is relatively independent of excitation energy and in the present calculations P_f was taken as a constant for the decays of $A + 3$ nuclei. Values of P_f were determined either from a comparison of cross sections for forming the same isomer by $2n$ and $3n$ evaporation reactions or from Γ_n / Γ_f systematics. For decays from the $A + 2$ to $A + 1$ nuclei the branching between fission

TABLE II. Sources for the experimental data used in the determination of fission barrier parameters. Sources for spallation data.

Residual nucleus	Reaction	Source	Reference
²³⁴ Pu	²³³ U(α , 3n)	Vandenbosch <i>et al.</i>	18
²³⁶ Pu	²³⁵ U(α , 3n)	Vandenbosch <i>et al.</i>	18
	²³⁵ U(α , 3n)	Bethune, Britt, and Erkkila	19
²³⁸ Pu	²³⁸ U(α , 4n)	Coleman	20
²³⁹ Pu	²³⁸ U(α , 3n)	Wing <i>et al.</i>	21
²³⁸ Am	²³⁷ Np(α , 3n)	Gibson	22
	²³⁹ Pu(d , 2n)	Gibson	22
²⁴⁰ Cm	²³⁹ Pu(α , 3n)	Glass <i>et al.</i>	23
²⁴² Cm	²⁴² Pu(α , 4n)	Glass <i>et al.</i>	23

and neutron emission was allowed to vary with excitation energy but the approximation $\Gamma_n/\Gamma_f = \Gamma_n/\Gamma_A$ was used. This approximation is reasonable for cases where E_A is significantly larger than E_B and gets around some difficulties associated with the underestimate of Γ_B at high energies in the present model. Γ_A and Γ_B are widths for penetrating the first and second peaks of the fission barrier, respectively. This point is discussed in more detail in Sec. II B below.

The spectrum of excitation energies populated in the $A + 1$ nucleus is obtained by assuming that each neutron is evaporated with a Maxwellian energy distribution

$$N(\epsilon) \propto \epsilon \exp(-\epsilon/T_{1,2,3}),$$

where $T_{1,2,3}$ are appropriate temperatures for the excitation energies involved in the evaporation of neutrons from the $A + 1$, $A + 2$, and $A + 3$ nuclei, respectively, and ϵ is the energy of the emitted neutron. In addition, for the initial reaction pre-equilibrium neutron emission is accounted for by adding a neutron-decay component whose shape and relative intensity are determined from the calculations of Blann.³² It is assumed that pre-equilibrium neutrons are emitted so rapidly that fission does not compete with these decays. The variation of the fraction of pre-equilibrium emission with energy is taken from the calculations of Blann but an over-all normalization factor is treated as an adjustable parameter in the fits. For the energy range important for $2n$ evaporation reactions the calculated fraction of pre-equilibrium emission is generally in the range 0.05 to 0.10.

TABLE III. Sources for the experimental data used in the determination of fission barrier parameters. Sources for fission-isomer half-lives.

Isomer	$T_{1/2}$ (sec)	Source	Reference
²³⁵ Pu	3×10^{-8}	Britt <i>et al.</i>	1
²³⁷ Pu	1.1×10^{-7}	{ Temperley <i>et al.</i> ; Russo <i>et al.</i>	24
	1.0×10^{-6}		
²³⁸ Pu	5×10^{-10}	Sletten and Limkilde	10
²³⁹ Pu	8×10^{-6}	Polikanov and Sletten	11
²⁴⁰ Pu	4×10^{-9}	Britt <i>et al.</i>	1
²³⁷ Am	5×10^{-9}	Polikanov and Sletten	11
²³⁸ Am	3.5×10^{-5}	Polikanov and Sletten	11
²³⁹ Am	1.6×10^{-7}	Lark <i>et al.</i>	14
²⁴⁰ Am	0.9×10^{-3}	Bjørnholm <i>et al.</i>	15
²⁴¹ Am	1.5×10^{-6}	Lark <i>et al.</i>	14
²⁴² Am	1.4×10^{-2}	Polikanov <i>et al.</i>	25
²⁴³ Am	6.5×10^{-6}	Polikanov and Sletten	11
²⁴⁴ Am	1.1×10^{-3}	Bjørnholm <i>et al.</i>	26
²⁴¹ Cm	1.5×10^{-8}	Britt <i>et al.</i>	1
²⁴³ Cm	3.8×10^{-8}	Polikanov and Sletten	11
²⁴⁵ Cm	2.3×10^{-8}	Britt <i>et al.</i>	1

TABLE IV. Sources for the experimental data used in the determination of fission barrier parameters. Sources for spontaneous-fission half-lives.

Ground state	$T_{1/2}$ (yr)	Source	Reference
²³⁸ Pu	5×10^{10}	Druin <i>et al.</i>	27
²³⁹ Pu	5.5×10^{15}	Segrè	28
²⁴⁰ Pu	1.4×10^{11}	Malkin <i>et al.</i>	29
²⁴¹ Am	2.3×10^{14}	Druin <i>et al.</i>	27
²⁴² Am	9×10^{11}	Caldwell <i>et al.</i>	30
²⁴³ Am	3.3×10^{13}	Aleksandrov <i>et al.</i>	31

2. Population of A Nucleus

For the relevant excitation energies the decay of the $A + 1$ nucleus is dominated by fission and neutron emission. Neglecting γ -ray deexcitation the excited $A + 1$ nucleus can decay by neutron emission to the A nucleus at either the normal (well I) or isomeric (well II) deformations or it can decay by prompt fission. In a strong coupling approximation these decay modes are governed by the widths for penetrating the two peaks of the fission barrier Γ_A^I , Γ_A^{II} , and Γ_B^{II} , and the neutron decay widths in the two equilibrium deformations, Γ_n^I and Γ_n^{II} . For convenience in calculating the isomer cross sections the effective number of decay channels for a particular mode, $N = 2\pi\Gamma/D$, is used where D is the level spacing in the appropriate well at the appropriate excitation energy. For the various decay modes

$$N_A = 2\pi\Gamma_A^I/D_I = 2\pi\Gamma_A^{II}/D_{II},$$

$$N_B = 2\pi\Gamma_B^{II}/D_{II},$$

$$N_I = 2\pi\Gamma_n^I/D_I,$$

and

$$N_{II} = 2\pi\Gamma_n^{II}/D_{II}.$$

If, as illustrated in Fig. 2, there is an initial population K of nuclei at some particular energy in well I in the $A + 1$ nucleus, the number of nuclei decaying by the three modes is given by:

(a) Decay to A nucleus in well I:

$$P_I = KN_I(N_A + N_{II} + N_B)/\alpha, \quad (1)$$

TABLE V. Single-particle potential parameters for ²⁴⁰Pu.

Neutron well depth V_n	45.2 MeV
Proton well depth V_p	59.8 MeV
Radius R_0 of spherical generating potential	7.94 fm
Yukawa range a	0.90 fm
Spin-orbit interaction strength λ	32.0

1. Determination of Single-Particle States

As the nucleus deforms, the density of single-particle states near the Fermi surface fluctuates strongly. This is responsible for similar fluctuations in the nuclear potential energy of deformation, such as the occurrence in actinide nuclei of deformed ground-state shapes and fission barriers that contain two peaks separated by a secondary minimum.

At the local minima in the potential energy the density of single-particle states is lower than average,^{7,8,34} which leads to compound-nuclear level densities that at low excitation energies are also lower than average. Conversely, local maxima in the potential energy correspond to higher than average single-particle level densities, and consequently to higher than average compound-nuclear level densities. However, when the total potential energy contains a high and sharp peak as a function of the symmetric fission coordinate, it is sometimes energetically favorable for the nucleus to go *around* rather than over the peak by taking advantage of asymmetric deformations. In particular, the energy at the second saddle point of some actinide nuclei is lowered by about 3 MeV by the introduction of reflection asymmetric deformations.³⁴⁻³⁶ This is because the single-particle contribution to the energy decreases more rapidly with reflection asymmetry than the liquid-drop contribution increases. In these cases the density of single-particle states, and hence, the compound-nuclear level density, is lower than average at the second saddle point in addition to the two minima.⁸ For some of the heavier actinide nuclei (but *not* the lighter ones) the energy of the first peak is lowered somewhat by axially asymmetric (γ) deformations,³⁶⁻³⁸ which are associated with a similar reduction in level densities at the first saddle point.

According to the transition-state method,^{39,40} the decay widths are functions of the compound-nuclear level densities evaluated at their extrema as a function of deformation. At low excitation energies these extrema occur approximately at the static equilibrium points in the nuclear potential energy of deformation, namely at the ground-state minimum, first saddle, secondary minimum, and second (asymmetric) saddle.⁴ We have used the approximation that the extrema in the compound level densities occur at these static equilibrium points, which is fairly good except at high excitation energies, where the extrema in the compound-nuclear level density shift toward the equilibrium configurations of the liquid-drop model.

The procedure is, therefore, to first calculate the nuclear potential energy as a function of de-

formation. This is done by means of the macroscopic-microscopic method applied to realistic diffuse-surface single-particle potentials, as discussed in detail in Ref. 8. In this method, the smooth trends of the potential energy are described by the liquid-drop model, and the local fluctuations by shell and pairing corrections calculated from a single-particle model. The parameters of the liquid-drop model are taken from the second mass formula of Myers and Swiatecki,⁴¹ and the parameters of the single-particle potential from the statistical model calculations of Myers.⁴² The resulting single-particle potential parameters for ²⁴⁰Pu are listed in Table V.

The nuclear shape is specified in terms of smoothly joined portions of three quadratic surfaces of revolution.^{8,43} This parametrization contains a total of five coordinates, of which three represent symmetric deformations and the remaining two represent reflection asymmetric deformations.

In some cases the equilibrium points were determined by imposing constraints upon some of the coordinates. This was done partly for computational simplicity and partly to test the sensitiv-

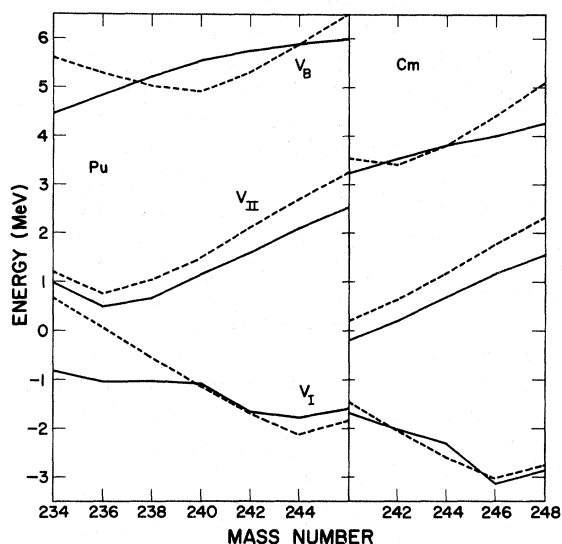


FIG. 3. Theoretical calculations of the potential energies at the first minimum, second minimum, and second maximum relative to the spherical liquid-drop energy. For V_I the dashed and solid curves are minima obtained allowing only spheroidal deformations and deformations somewhat more diamond-like than spheroidal, respectively. For V_{II} the dashed and solid curves are for minima calculated in the restricted γ family of shapes and by varying the three symmetric distortions, respectively. For V_B the dashed and solid curves are saddle points obtained using the saddle point shape for ²⁴⁰Pu and by varying the γ and α_2 coordinates, respectively.

TABLE VI. Results from fits to experimental data using alternate sets of single-particle levels. V_B is the calculated energy relative to the spherical liquid-drop energy, and E_{shell} is the calculated value of the shell correction. E_{II} and E_B are deduced from fits to experimental data. Comparison of fits with levels of the spheroidal and diamond-like minima in the first well for ^{243}Cm and ^{245}Cm .

	^{243}Cm		^{245}Cm	
	Diamond-like minimum	Spheroidal minimum	Diamond-like minimum	Spheroidal minimum
V_B (MeV)	-2.01	-1.95	-2.30	-2.49
$E_{B \text{ shell}}$ (MeV)	-4.21	-3.34	-4.01	-4.02
E_{II} (MeV)	1.50	1.70	1.70	1.70
E_B (MeV)	4.00	4.10	4.40	4.40

ity of the final results to different level densities arising from the use of different constraints. The effects of some of these constraints on the energies of plutonium and curium isotopes are illustrated in Fig. 3. The energy V_I at the ground-state minimum was calculated first for pure spheroidal deformations (lower dashed curves) and second by varying all three symmetric coordinates, but under the constraint that the shapes be somewhat more diamond-like than a spheroid (lower solid curves). For the lighter plutonium isotopes the true diamond-like ground-state minimum is substantially lower in energy than the spheroidal minimum and consequently was used in the level-density calculation. In the other cases the energies are roughly comparable, and studies were made with single-particle levels obtained at each minimum to see the effect of the constraints.

Although the total energy near an extremum depends quadratically upon shape deviations and is consequently relatively flat, the individual liquid-drop energy, shell correction, and pairing correction depend linearly and consequently can differ substantially for different shapes. Because the single-particle level density is correlated with the shell correction, the largest differences in the extracted barrier parameters occur when the values of the shell correction differ most. This is illustrated in Table VI, where it is seen that a difference of 0.87 MeV in the value of the shell correction for ^{243}Cm leads to a difference of 0.20 MeV in the extracted value of E_{II} and to a difference of 0.10 MeV in the extracted value of E_B . For

^{245}Cm , where the shell corrections at the two minima are approximately equal, the extracted barrier parameters are identical.

The middle dashed curves in Fig. 3 give the energy V_{II} at the secondary minimum calculated for the one-dimensional γ family of shapes of Ref. 8. Single-particle levels corresponding to these shapes were used in the studies reported here. When the remaining two symmetric coordinates are taken into account, the energy of the secondary minimum is reduced somewhat as shown by the middle solid curves. However, some calculations performed with levels corresponding to these shapes indicate that the final barrier parameters change by less than 0.1 MeV. Single-particle levels calculated for the γ family of shapes were also used at the first saddle point. At the first saddle modifications of the single-particle level spectra due to the axially asymmetric (γ) deformation³⁶⁻³⁸ were neglected.

At the second (asymmetric) saddle point a somewhat more severe approximation was employed, owing to the difficulty of simultaneously varying five coordinates. The saddle point shape for ^{240}Pu was determined in Ref. 8 by first varying the three symmetric coordinates to locate the symmetric peak, and then varying the mass asymmetry coordinate

$$\alpha_2 = \frac{a_1^2 - a_2^2}{\frac{1}{2}(a_1^2 + a_2^2)},$$

where a_1 and a_2 are the transverse semi-axes of the left-hand and right-hand spheroids forming the

TABLE VII. Results from fits to experimental data using alternate sets of single-particle levels. V_I is the calculated energy relative to the spherical liquid-drop energy, and E_{shell} is the calculated value of the shell correction. E_{II} and E_B are deduced from fits to experimental data.

	^{240}Pu levels	Alternate set I	Alternate set II
V_I (MeV)	5.59	3.93	4.91
$E_{I \text{ shell}}$ (MeV)	-1.60	-1.61	-0.03
E_{II} (MeV)	1.70	1.60	1.85
E_B (MeV)	4.60	4.60	4.85

shape. The single-particle levels corresponding to this one shape were used for the second saddle point in the studies reported here. The total energies of the plutonium and curium isotopes corresponding to this shape are given by the upper dashed curves in Fig. 3. The upper solid curves give the energies calculated by simultaneously varying the approximate fission coordinate y and the mass asymmetry coordinate α_2 . To test the sensitivity of the final barrier parameters to the single-particle levels at the second saddle point, some calculations were performed for ^{235}Pu with two alternate sets of levels corresponding to different shapes at the second saddle point. As indicated in Table VII, the final barrier parameters differ at most by 0.25 MeV, which corresponds to an extreme variation of 1.57 MeV in the value of the shell correction.

2. Calculation of Compound-Nuclear Level Density

Once the single-particle spectra are known, the compound-nuclear-state density can be calculated by applying the method of steepest descents (the saddle-point integral method) according to the basic formula⁴⁴

$$\rho(E, N, Z) = \frac{1}{(2\pi i)^3} \iint_{-i\infty}^{i\infty} e^{\beta(E - \lambda_n N - \lambda_p Z)} \times \text{Tr}[e^{-\beta(\hat{H} - \lambda_n \hat{N} - \lambda_p \hat{Z})}] \beta^2 d\beta d\lambda_n d\lambda_p, \quad (4)$$

where \hat{N} and \hat{Z} are the particle-number operators corresponding to N and Z . In the particular set of states used to evaluate the trace, ρ takes the form

$$\rho(E, N, Z) = \frac{1}{(2\pi i)^3} \iint_{-i\infty}^{i\infty} e^{S(\beta, \lambda_n, \lambda_p)} d\beta d\lambda_n d\lambda_p,$$

and the method of steepest descents gives

$$\rho(E, N, Z) \approx (2\pi)^{-3/2} \det \left[\left(\frac{\partial^2 S}{\partial \mu_i \partial \mu_j} \right)_0 \right]^{-1/2} e^{S_0}.$$

Here μ_i takes the values β , λ_n , and λ_p . The subscript 0 indicates that the μ_i take the values that maximize S , so that

$$\frac{\partial S}{\partial \mu_i} = 0, \quad \mu_i = \mu_{i0}.$$

The maximum value of S is S_0 .

The pairing correction is applied to the single-particle spectra by means of a method similar to that used by Decowski *et al.*⁶ It is assumed that the pairing interaction couples neutron pairs or proton pairs, but not neutron-proton pairs. Then

$\hat{H} - \lambda_n \hat{N} - \lambda_p \hat{Z}$ splits into a neutron term $\hat{H}_n - \lambda_n \hat{N}$ and a similar proton term. Each of these terms is treated separately in the BCS approximation. The relevant equation for computing the trace is

$$\text{Tr}[e^{-\beta(\hat{H} - \lambda \hat{N})}] = e^{-\beta F_0} \prod_{\nu} (1 + e^{-\beta E_{\nu}})^2, \quad (5)$$

where E_{ν} is the quasiparticle energy

$$E_{\nu} = (f_{\nu}^2 + \Delta^2)^{1/2}.$$

The quantities f_{ν} and Δ are obtained by solving the gap equation

$$1 = \frac{G}{2} \sum_{\nu} \frac{1}{E_{\nu}} \tanh \left(\frac{\beta E_{\nu}}{2} \right),$$

together with the equation

$$f_{\nu} = \epsilon_{\nu} - \lambda - \frac{G}{2} + \frac{G}{2} \frac{f_{\nu}}{E_{\nu}} \tanh \left(\frac{\beta E_{\nu}}{2} \right), \quad (6)$$

where G is the pairing interaction strength taken from the single-particle calculations. The last two terms in the preceding equation are often neglected as being of higher order^{4,6}; however, they do appear in the first approximation and are easily included in the program. In Eq. (6), ϵ_{ν} is the single-particle energy computed without pairing. The quantity F_0 in Eq. (5) is the ground-state energy for the appropriate values of β and λ . It is given by

$$F_0 = \frac{1}{2} \sum_{\nu} \left[E_{\nu}(t_{\nu} - 2) + 2e_{\nu} + \frac{G}{2} - \frac{e_{\nu}^2 t_{\nu}}{E_{\nu} - (G/2)t_{\nu}} \right],$$

where

$$t_{\nu} = \tanh \left(\frac{\beta E_{\nu}}{2} \right)$$

and

$$\epsilon_{\nu} = \epsilon_{\nu} - \lambda - \frac{G}{2}.$$

For given values of λ_n , λ_p , and β , the BCS equations are solved and S is computed. The λ 's and β are varied until the maximum value of S is obtained. The second derivatives are found by taking differences, and ρ is obtained from Eq. (4).

The compound-state densities calculated above contain states of all angular momenta and both parities. The density of compound levels of a particular spin and parity was obtained by normalizing to the known density of 1^+ states from ^{240}Pu at the neutron binding energy and then applying a standard statistical spin-distribution function² with spin-cutoff factor $\sigma = 5.45$ MeV to obtain densities of levels with arbitrary J . It was assumed that both parities were equally probable. Actually the calculated isomer excitation functions were not sensitive to the spin distribution of initial states or to the normalization of the level densities and

these considerations are important only in comparing calculated level densities with neutron-resonance measurements for the various cases.

The calculations described above are all for even-even nuclei but in the isomer calculations level densities for even-odd and odd-odd nuclei are also necessary. Level-density functions for odd- A and odd-odd nuclei were approximated by using the calculated functions for even-even nuclei and shifting the excitation-energy scales by Δ_n and/or Δ_p .

Results for compound-nuclear-level-density calculations at the first minimum and the first saddle for ^{240}Pu are shown in Figs. 4 and 5. In Fig. 4 the energies are plotted relative to the energy of the lowest state in the unpaired system, and it is seen that in this reference system the level densities are always higher at the first saddle. In this reference system the results are qualitatively similar to Fermi-gas distributions with $a_f > a_n$. However, when the calculations are done including pairing effects it is seen that the condensation energy is larger for the more dense single-particle levels at the first maximum than for the more widely spread levels at the first minimum. As a result when the level densities are plotted as a function of the energy above the lowest paired state (i.e. normal excitation energy) the level densities at the first minimum at low energies are actually higher than those at the first maxima (see Fig. 5). The level-density dependence shown in Fig. 5 is not approximated very well by the generalized Fermi-gas functions or by the generalized Gilbert and Cameron function used in Ref. 1. It should be

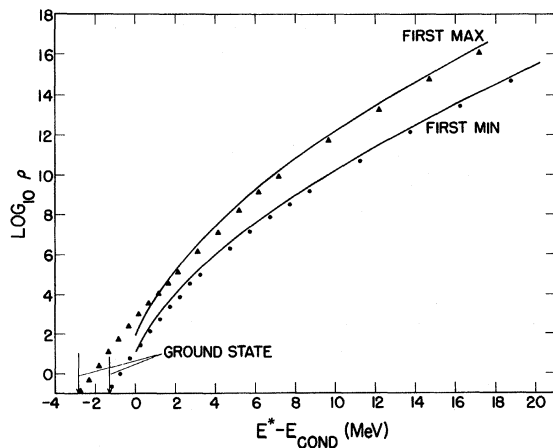


FIG. 4. Calculations of the total compound level density as a function of the excitation energy relative to the unpaired ground state for the first minimum and first maximum of ^{240}Pu . Solid curves are calculations with no pairing. Dots and triangles are similar calculations including the pairing interaction.

remembered, however, that these calculations do not consider possible γ instabilities at the first saddle. The effect of an equilibrium γ deformation at this first saddle would be to decrease the shell energy, the density of single-particle states near the Fermi surface, and the pairing condensation energy.

3. Calculation of Γ_n/Γ_A

Using the relationships given in Appendix A of Ref. 1 with compound level densities from appropriate single-particle-level spectra as described in the previous two sections it is possible to calculate decay widths for neutron decay, fission, and γ -ray emission. Of particular interest are calculations of Γ_n/Γ_f and comparison of these calculations with experimental information from various sources.

From Eqs. (1) and (3) in Sec. II A 2 when the effects of decay to the isomeric well are neglected it is seen that Γ_n/Γ_f can be expressed as

$$\frac{\Gamma_n}{\Gamma_f} = \frac{\Gamma_n}{\Gamma_A} \left(\frac{\Gamma_A + \Gamma_B}{\Gamma_B} \right).$$

For most of the cases considered here E_A is greater than E_B , and at low excitation energies $\Gamma_B \gg \Gamma_A$. The approximation

$$\frac{\Gamma_n}{\Gamma_f} \approx \frac{\Gamma_n}{\Gamma_A}$$

is therefore adequate for most purposes. However, in the present model at high excitation energies the calculations give $\Gamma_B < \Gamma_A$ indicating that the liquid-drop energy surface at the deformation corresponding to the second *asymmetric* saddle is

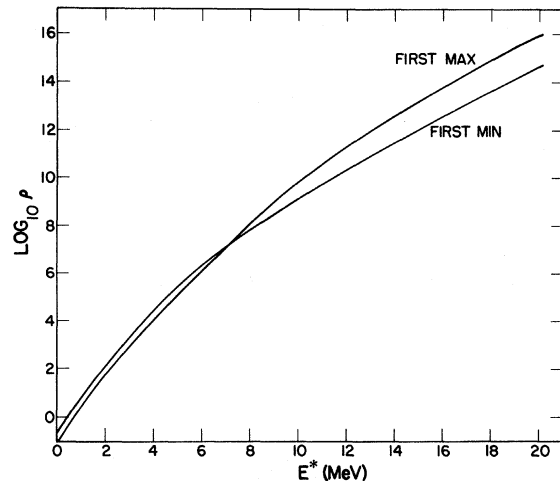


FIG. 5. Calculations of the total compound level density as a function of excitation energy for the first minimum and first maximum of ^{240}Pu .

higher than at the first saddle. Part of this effect is artificial because of the assumption that the position of the second saddle point is independent of excitation energy when in fact at $E^* > 20$ MeV the level densities at the second symmetric saddle become larger than those at the asymmetric saddle even though the symmetric saddle is somewhat higher. In the present calculations since we do not adequately treat the possibility of the nucleus passing over barrier B with a range of possible asymmetric distortions and the determination of the asymmetric saddle itself is rather uncertain, it was decided to use the approximation $\Gamma_n/\Gamma_f \approx \Gamma_n/\Gamma_A$ for the excitation energies encountered in the $A+2$ nucleus. This will tend to underestimate Γ_n/Γ_f in the decay of the $A+2$ nucleus but it is believed that the effect on the final barrier parameters is small compared to other uncertainties in the model.

To illustrate some of the general characteristics of the Γ_n/Γ_A calculations, Fig. 6 shows results for ^{241}Pu and ^{235}Pu for a variety of different conditions. The peak in Γ_n/Γ_A at 4–5 MeV is a result of the crossing of $\rho(E^*)$ shown in Fig. 5 and this is a result of the difference in pairing at the minimum and maximum. This is seen in the comparison with the calculation which ignores pairing. The neglect of pairing effects also underestimates

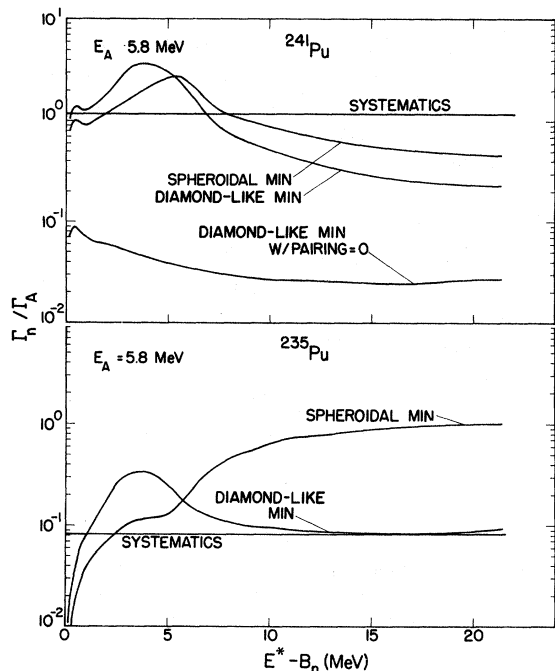


FIG. 6. Calculations of Γ_n/Γ_A for ^{241}Pu and ^{235}Pu with various sets of single-particle levels. The values labeled "systematics" are empirical values of Γ_n/Γ_f from Ref. 45. In both cases the value $E_A = 5.8$ MeV was used.

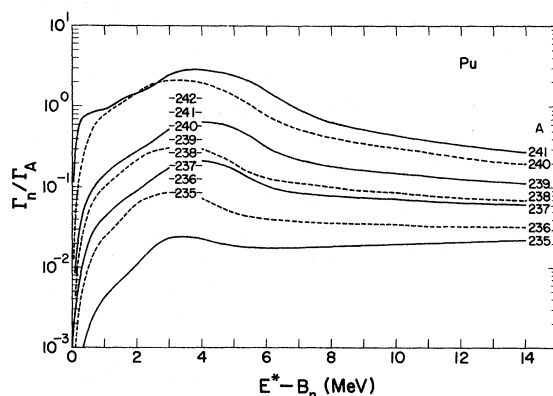


FIG. 7. Calculations of Γ_n/Γ_A for a series of plutonium isotopes. Numbers with accompanying dashes in the center of the figure indicate empirical values of Γ_n/Γ_f from Ref. 45. The calculated values used for E_A in each case are listed in Table IX.

Γ_n/Γ_A by approximately an order of magnitude because of the difference in pairing condensation energies at the minimum and maximum. It is also seen that the use of single-particle levels from the diamond-like minimum, where a positive hexadecapole distortion is allowed, changes the calculations significantly. The change is largest for ^{235}Pu , where the equilibrium hexadecapole distortion is largest. In general, for a reasonable assumption about the height of the first saddle ($E_A = 5.8$ MeV), the calculated values for Γ_n/Γ_A are similar to values obtained from empirical systematics.⁴⁵

Figure 7 shows calculated values for Γ_n/Γ_A using values for E_A from the theoretical single-particle calculations (given later in Table IX). In general the average calculated values agree reason-

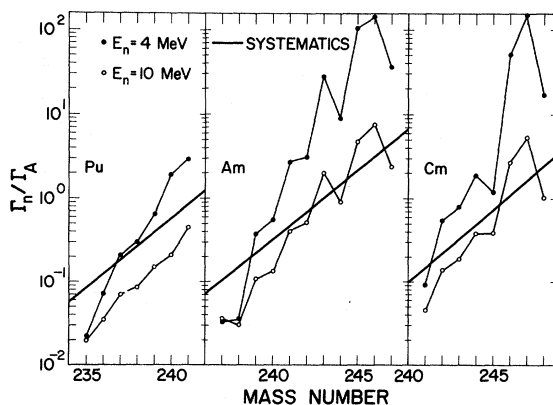


FIG. 8. Calculations of Γ_n/Γ_A as a function of mass number for a series of plutonium, americium, and curium isotopes. Solid lines represent the empirical values of Γ_n/Γ_f from Ref. 45.

ably well with empirical systematics⁴⁵ except that the change in Γ_n/Γ_A with mass number is too rapid. This discrepancy is due to the too rapid variation of E_A from the theoretical calculation. These results and similar calculations for americium and curium nuclei are also shown in Fig. 8 and again it is seen that the theoretical calculations reproduce experimental systematics⁴⁵ reasonably well except for a too rapid variation with mass number.

For several of the plutonium isotopes Γ_n/Γ_A calculations were also performed using single-particle levels calculated with a harmonic-oscillator potential by Tsang *et al.*⁴⁶ These results gave substantially the same features as obtained using levels from the present diffuse-surface potential.

C. Determination of Parameters and Tests of Model Calculations

1. Nuclear Temperatures

In a completely self-consistent model the spectrum of excitation energies populated following the emission of a neutron at each stage of the evaporation can be determined simply from the energy dependence of the compound level density in the residual nucleus. When this self-consistent approach was tried it was found that fits to experimental data did not give the same values for E_{II} from data for the $^{235}\text{U}(\alpha, 2n)^{237m}\text{Pu}$ and $^{236}\text{U}(\alpha, 3n)^{237m}\text{Pu}$ reactions and did not agree well with the known threshold for the ground-state reaction $^{235}\text{U}(\alpha, 3n)^{236}\text{Pu}$.

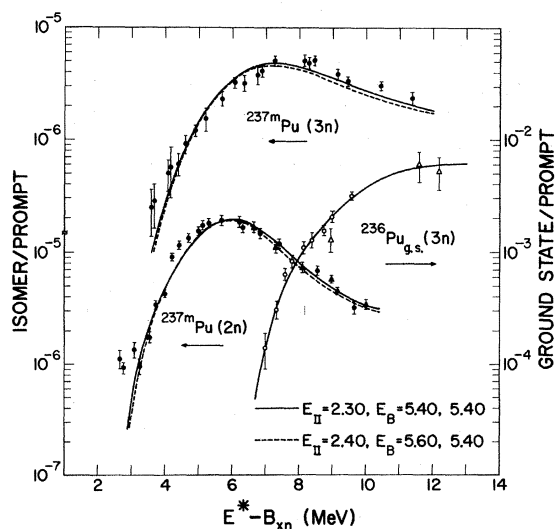


FIG. 9. Fits to experimental data for the production of the ^{237m}Pu isomer by (2n) (Ref. 1) and (3n) (Ref. 9) evaporation reactions and for the production of ^{236}Pu at its ground-state deformation by a (3n) evaporation reaction (Ref. 19). The values of the parameters E_{II} and E_B are given for each of two equivalent fits with the two E_B values referring to the $A+1$ and A nuclei, respectively.

Because of this difficulty the completely self-consistent approach was abandoned and instead it was assumed that the neutrons were evaporated with a Maxwellian energy spectrum whose shape was determined by an empirical nuclear temperature. The empirical nuclear temperatures were determined by simultaneous fits to the excitation functions for producing the ^{237m}Pu fission isomer from 2n and 3n evaporation reactions and the excitation function for the $^{235}\text{U}(\alpha, 3n)^{236}\text{Pu}$ ground-state reaction. The comparison of the 2n and 3n reactions gives an average temperature in the $A+2$ nucleus. The ground-state ^{236}Pu excitation function is sensitive to the sum of the two temperatures in the A and $A+1$ nuclei. The fits to experimental data are shown in Fig. 9 and the empirical nuclear temperatures in Table VIII along with the theoretical nuclear temperatures at the appropriate average excitation energies from the single-particle levels described in Sec. IIB and from single-particle levels calculated by Tsang *et al.*⁴⁶

From Table VIII it is seen that the experimental temperatures are less than those determined from the compound level densities. This may indicate that either the temperatures from the level densities are too high and/or that the "experimental" temperatures are coming out too low in order to compensate for inadequacies in the energy dependence of the Γ_n/Γ_f calculations. For example, the neglect of γ deformations at the first saddle could lead to systematic errors in the low energy behavior of Γ_n/Γ_f . In all of the fits presented below the nuclear temperatures were held fixed at the values given in Table VIII.

2. Effects of Pre-Equilibrium Emission

As described in Sec. IIA the shapes of the pre-equilibrium neutron spectra and the fraction of the total reaction cross section going into the pre-equilibrium component at each excitation energy were taken from Blann.³² The calculated isomer excitation functions were not significantly dependent on the choice of incident particle in the pre-equilib-

TABLE VIII. Effective nuclear temperatures determined from comparison of experimental data to model calculations and theoretical estimates from the compound level density using single-particle levels from the present calculations and from calculations by Tsang (Ref. 46).

Nucleus	Average E^* (MeV)	T (experimental) (MeV)	T (theoretical) (MeV)	
			Present results	Tsang
A	5	0.4 ± 0.1	0.52	0.47
$A+1$	11	0.5 ± 0.1	0.74	0.68
$A+2$	17	0.6 ± 0.1	0.91	0.84

rium calculations and for all cases results appropriate for α -particle reactions were used although tests were also performed using calculations for proton reactions. This relative insensitivity to the initial particle-hole number in the pre-equilibrium evaporation is also apparent in the experimental results where in many cases isomer/prompt ratios from $(\alpha, 2n)$, $(p, 2n)$, and $(d, 2n)$ reactions agree very well.

Figure 10 shows the sensitivity of the calculated fission-isomer excitation functions to variations in the fraction of the cross section going into pre-equilibrium emission. It is seen that the pre-equilibrium component is qualitatively more important for ^{235m}Pu where Γ_n/Γ_f is small for the first neutron evaporation. In addition, Fig. 10 shows the effect of multiplying the theoretical pre-equilibrium component by 0.5 and 2.0. In the fits to be described in Sec. III it was found that a good representation of the high-energy portion of the fission-isomer excitation functions could be obtained for most cases with values for the intensity of the pre-equilibrium component that were in the range 0.5–2.0 times the theoretically calculated values.³²

The shape of the high-energy portion of the excitation functions is also sensitive to other parameters in the model, to the assumptions made about coupling between the levels in the two wells, and to the shape of the spectrum of emitted neutrons. For this reason the values obtained for the pre-equilibrium component in specific cases are prob-

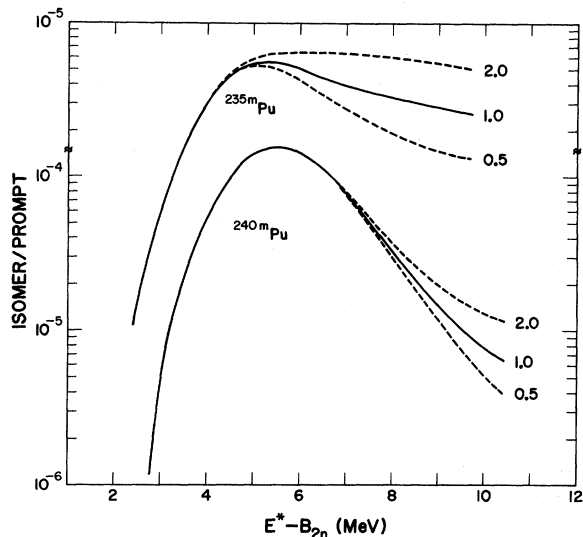


FIG. 10. Effect of changing the percentage of pre-equilibrium emission on the calculated fission-isomer excitation functions for ^{235m}Pu and ^{240m}Pu . Curves show the results of multiplying the theoretically estimated percentages of pre-equilibrium emission by 0.5, 1.0, and 2.0.

ably not very significant. Instead the fact that most of the excitation functions can be fitted with values for the pre-equilibrium component that are within a factor of 2 of the theoretically calculated values simply helps to confirm the validity of the present statistical model.

In general the parameters obtained from the fits to experimental data are not very sensitive to the details of the pre-equilibrium emission and the inclusion of this effect in the present model just gives an improved representation of the high-energy portions of the excitation functions.

3. Ambiguities in Parameter Values

Once the temperatures and the prescription for the calculation of the pre-equilibrium components are fixed the major parameters which remain in the model are:

- (1) E_A values for all of the nuclei involved in a particular reaction,
- (2) E_B values for the A and $A + 1$ nuclei, and
- (3) E_{II} values for the A nucleus.

From studies of fits with different assumptions about the relationships between the various parameters it was found that in most cases there was a considerable range of parameters which could be found to give equivalent fits to the experimental data. Therefore, an entire set of barrier parameters could not be obtained from a fit to a single fission-isomer excitation function and outside sources had to be relied on for some of the parameters.

In general, adequate fits to the experimental isomer excitation functions could be obtained with any reasonable choice of heights for the first barrier E_A . However, large differences in the choices of the E_A values resulted in compensating changes in the fitted values for E_B and E_{II} . As was shown in Sec. II B 3 the theoretical values for E_A lead to predictions for Γ_n/Γ_A that are in reasonable agreement with experimental systematics. Since the theoretical values are the only set which cover the entire range of nuclei of interest, this set was used in the first fits to all the experimental data. For the americium nuclei a series of experimental values for the height of the first barriers have recently become available from direct-reaction fission experiments^{47, 48} and these barriers were used for a second set of fits to fission-isomer data for ^{238m}Am through ^{243m}Am . In the future it is expected that experimental values of E_A will be available⁴⁸ for many more of the plutonium and curium isotopes, but since this work is not yet complete, fits to isomer data in this region were not attempted with experimental barriers. A further discussion of the effect of the choice of E_A

values on the other parameters is given in Sec. III below.

The calculated fission-isomer excitation functions are sensitive to the height of the second peak E_B in both the A and $A+1$ nuclei, but it is not possible to determine both barrier heights from the fit to a single excitation function. This ambiguity is illustrated for the ^{237m}Pu isomer fits in Fig. 9. For definiteness all of the isomer data were fitted assuming $E_B(A+1) = E_B(A)$, which should be a good assumption in cases where E_B is not changing rapidly with A . In the americium nuclei, where there does appear to be a strong odd-even effect in the E_B values, an additional set of fits were obtained with the requirement that the E_B values used in the fits be consistent for isomers in adjacent nuclei.

As described in the previous paper,¹ the calculations of Γ_A and Γ_B also require values for $\hbar\omega_A$ and $\hbar\omega_B$ but the results are not very sensitive to the values chosen. For the fits described in this paper $\hbar\omega$ values were taken from the analysis of Back *et al.*⁴⁷

4. Sensitivity to Single-Particle Level Spectra

In addition to the dependence of the calculations on the parameters discussed above, the results are also dependent on the choice of the single-particle level spectrum used in calculating the appro-

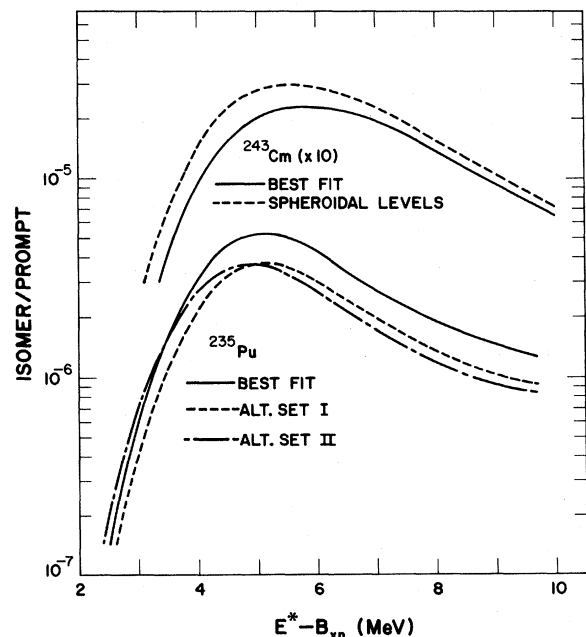


FIG. 11. Effect of changing the single-particle level spectra on the calculated fission-isomer excitation functions for ^{235}Pu and ^{243}Cm . Details of the single-particle spectra are given in the text and in Tables VI and VII.

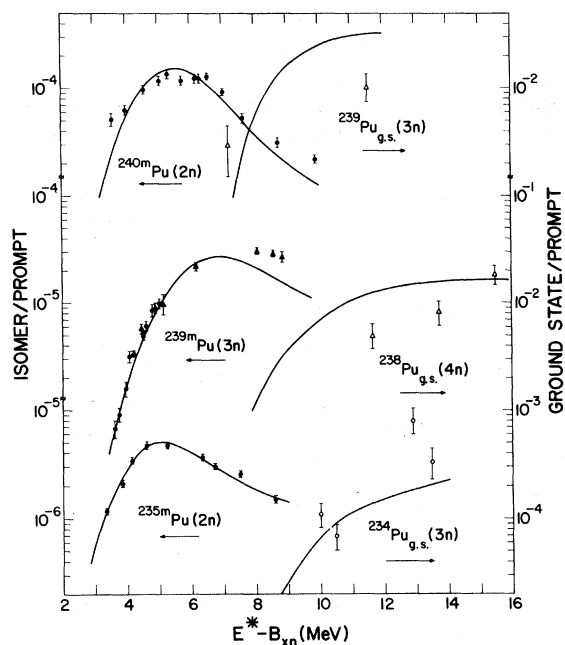


FIG. 12. Fits to fission-isomer and ground-state spallation excitation functions. References to experimental data are given in Table I-IV.

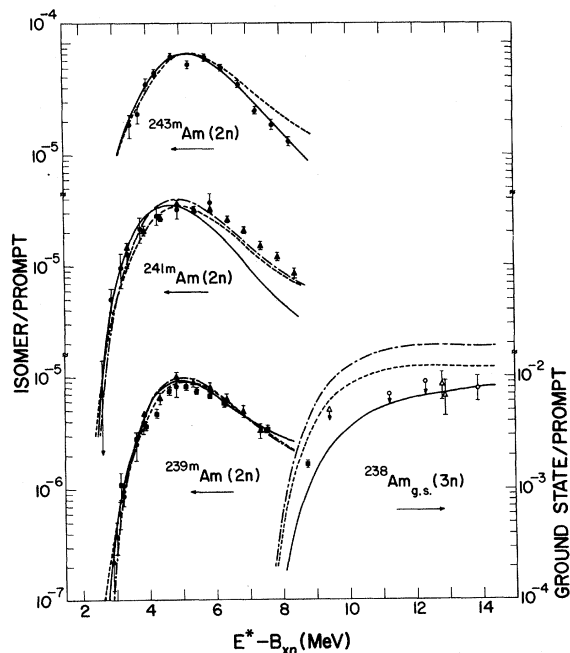


FIG. 13. Fits to fission-isomer and ground-state spallation excitation functions. References to experimental data are given in Tables I-IV. Solid curves are fits with calculated E_A values with $E_B(A+1) = E_B(A)$. Dashed curves are fits with experimental E_A values with $E_B(A+1) = E_B(A)$. Dot-dashed curves are fits with experimental E_A values with $E_B(A+1) \neq E_B(A)$.

appropriate decay widths. As was discussed in Sec. II B 1, there is some difficulty in finding the true minimum in the first well for $N \geq 146$ and in determining the position of the second saddle for all nuclei. In order to test the uncertainties in the barrier parameters due to uncertainties in the single-particle level spectra, independent fits were made to the ^{235m}Pu isomer data with alternate level spectra at the second maximum and to ^{243m}Cm and ^{245m}Cm with level spectra at the first minimum which correspond to both the diamond-like minimum and the spheroidal minimum. The calculated excitation functions for ^{235m}Pu and ^{243m}Cm with all parameters the same except for the single-particle level spectra are shown in Fig. 11, and the E_{II} and E_B parameters obtained when the experimental results are refitted using the alternate level spectra are shown in Tables VI and VII. For ^{235}Pu the alternate level spectra include the spectrum⁸ at the second saddle for ^{240}Pu and two alternate spectra which cover the region of maximum credible deviation from this set for all nuclei. The results shown in Table VII indicate a maximum change of

0.2 and 0.25 MeV in E_{II} and E_B values due to changes in the assumed single-particle levels. For the fits described in the following section the ^{240}Pu levels at the second asymmetric maximum were used.

III. FITS TO EXPERIMENTAL DATA

A. E_{II} and E_B from Isomer Excitation Functions

Using the statistical model, as described in the preceding section, fits were performed to all available data on fission-isomer excitation functions in plutonium, americium, and curium nuclei. In these fits values for $E_{\text{II}}(A)$, $E_B(A+1)$, and $E_B(A)$ were determined. In addition, predictions for the population of the $A-1$ nucleus in its ground-state deformation were compared to spallation data wherever possible. The fits to experimental data are shown in Figs. 9 and 12–16, and the fission-barrier parameters are listed in Table IX.

1. Plutonium Nuclei

For the plutonium nuclei a complete set of experimental values for the first peak are not yet available, so the fits were performed using only the calculated E_A values. In addition there is no evi-

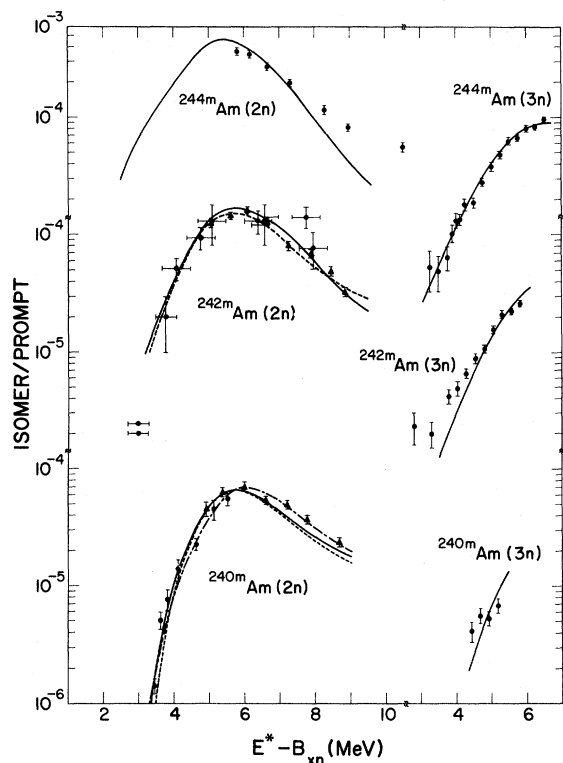


FIG. 14. Fits to fission-isomer excitation functions. References to experimental data are given in Tables I–IV. Solid curves are fits with calculated E_A values with $E_B(A+1) = E_B(A)$. Dashed curves are fits with experimental E_A values with $E_B(A+1) = E_B(A)$. Dot-dashed curves are fits with experimental E_A values with $E_B(A+1) \neq E_B(A)$.

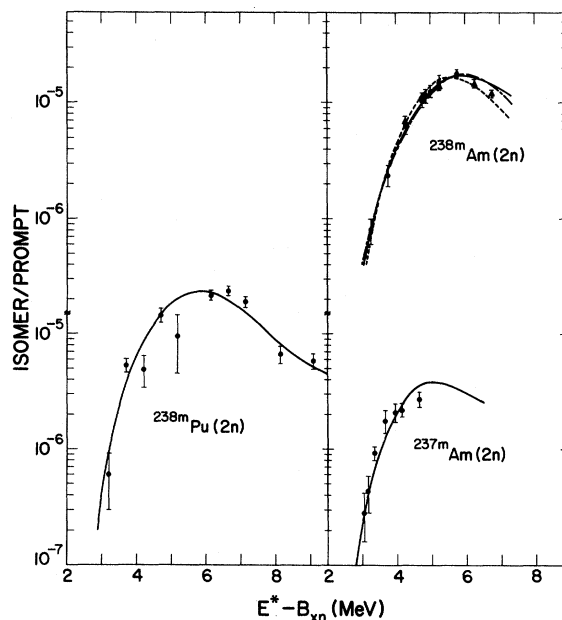


FIG. 15. Fits to fission-isomer excitation functions. References to experimental data are given in Tables I–IV. Solid curves are fits with calculated E_A values with $E_B(A+1) = E_B(A)$. Dashed curves are fits with experimental E_A values with $E_B(A+1) = E_B(A)$. Dot-dashed curves are fits with experimental E_A values with $E_B(A+1) \neq E_B(A)$.

dence for a strong dependence of E_B on mass number between ^{237}Pu and ^{240}Pu so that the fits were performed with the assumption $E_B(A+1) = E_B(A)$. For ^{235}Pu the value of E_B has decreased considerably but because there do not exist any data on the lowest isomer in ^{236}Pu the assumption $E_B(A+1) = E_B(A)$ had to be used again.

The prediction for the $^{235}\text{U}(\alpha, 3n)^{236}\text{Pu}$ excitation function was multiplied by a factor of 0.86 to get the best agreement with the experimental data. Because of the much poorer quality of the experimental data the calculated ground-state excitation functions for ^{235}Pu , ^{238}Pu , and ^{239}Pu (see Fig. 12) were not adjusted to give optimum fits. The trends apparent in Fig. 12 suggest that the calculations are giving cross sections for populating the $A-1$ nucleus that are systematically too small for ^{234}Pu and too large for ^{239}Pu with very good agreement for ^{237}Pu . This trend is consistent with results for americium nuclei (see below) where it is found that the calculated E_A values tend to increase too rapidly with neutron number compared to experimental measurements with agreement between the theoretical and experimental barriers occurring in the region of $N \approx 146$. A decrease of 0.1 MeV in all of the E_A values used in the $^{235}\text{U}(\alpha, 3n)^{236}\text{Pu}$ calculation leads to a decrease in the predicted cross section of $\approx 20\%$.

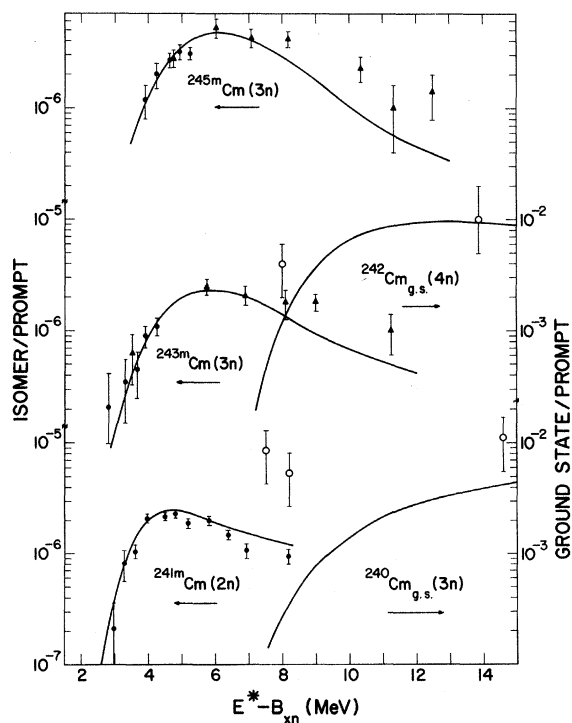


FIG. 16. Fits to fission-isomer excitation functions. References to experimental data are given in Tables I-IV.

2. Americium Nuclei

For the americium nuclei both experimental and theoretical values for the height of the first barrier are available and both sets were used in independent fits to the experimental excitation functions. The fits showed a strong odd-even dependence in E_B which was correlated with a similar effect in the experimental E_A values.⁴⁸ For this reason independent fits were made both with the assumption $E_B(A+1) = E_B(A)$ and with a set of E_B values correlated from nucleus to nucleus. The fits obtained with these three approaches are shown in Figs. 13-15, and parameters for each case are listed in Table IX with the "best" values underlined. The results in Table IX show that changes in the fitted parameters are usually within the range ± 0.20 MeV except for ^{239}Am and ^{240}Am where E_B values changed by 0.40 and 0.30 MeV, respectively, when the assumption $E_B(A+1) = E_B(A)$ was eliminated. These results and the studies with different sets of single-particle levels led to the assignment of ± 0.20 MeV estimated uncertainties on the parameters E_B and E_A determined from fits to experimental data. In Fig. 13 it can be seen that the best parameter set [experimental E_A values and $E_B(A+1) \neq E_B(A)$] tend to give superior fits to the experimental data indicating that improved experimental measurements might help to discriminate between parameter sets which must presently be considered equivalent.

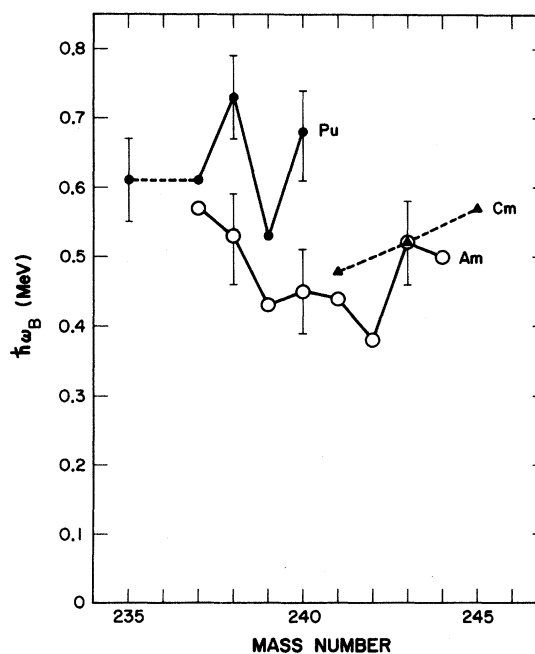


FIG. 17. Values for $\hbar\omega_B$ determined from fission-isomer half-lives.

TABLE IX. Barrier parameters determined from the analysis of experimental data. References to experimental data are contained in Tables I-IV. Dots for $E_B(A+1)$ indicate cases where $E_B(A) = E_B(A+1)$ was assumed. The "best" values are underlined.

Nucleus	E_A		E_{II} (MeV)	$E_B(A)$ (MeV)	$E_B(A+1)$ (MeV)	Isomer fission		Spontaneous fission		Direct reaction	Preequilibrium factor	$P_f(3n)$
	Calc. (MeV)	Expt. (MeV)				$T_{1/2}$ (sec)	$\hbar\omega_B$ (MeV)	$T_{1/2}$ (yr)	$\hbar\omega_A$ (MeV)	$\hbar\omega_A$ (MeV)		
^{235}Pu	4.70		1.70	4.60	...	3×10^{-8}	0.61				0.5	
^{236}Pu	5.04											
^{237}Pu	5.27		2.30	5.40	...	1×10^{-6}	0.59				0.5 (2n)	0.65
						1×10^{-7}	0.63				2.0 (3n)	
^{238}Pu	5.26		2.40	5.35	...	5×10^{-10}	0.73	5×10^{10}	0.83		1.0	
^{239}Pu	5.48	6.27 ^a	2.20	5.15	...	8×10^{-6}	0.53	5.5×10^{15}	0.82	0.78 ^c	2.0	0.56
^{240}Pu	5.49	6.00 ^{a b}	2.40	5.35	...	4×10^{-9}	0.68	1.4×10^{11}	0.89	1.00 ^c	2.0	
^{241}Pu	5.71	5.95 ^c	2.00 ^d							1.00 ^c		
^{242}Pu	6.20	6.10 ^a								1.00 ^c		
^{243}Pu	6.48	5.70 ^c	1.80 ^d							0.70 ^c		
^{244}Pu	6.43											
^{245}Pu		5.50 ^d	2.40 ^d									
^{237}Am	5.09		2.10	4.80	...	5×10^{-9}	0.57					
^{238}Am	5.33		2.40	5.35	...						0.5	
		6.40 ^e	2.50	5.15	...						0.5	
		<u>6.40^e</u>	<u>2.30</u>	<u>5.40</u>	4.60	3.5×10^{-5}	0.53				0.5	
^{239}Am	5.49		2.30	4.60	...						2.0	
		5.80 ^c	2.10	4.65	...						1.0	
		<u>5.80^c</u>	<u>2.50</u>	<u>4.65</u>	5.60	1.6×10^{-7}	0.43			0.75 ^c	1.0	
^{240}Am	5.71		2.70	5.20	...						2.0	
		6.45 ^c	2.90	5.25	...						2.0	
		<u>6.45^c</u>	<u>2.60</u>	<u>5.50</u>	4.50	9×10^{-4}	0.45			0.75 ^c	2.0	0.20
^{241}Am	6.01		2.10	4.35	...						2.0	
		5.70 ^c	2.00	4.55	...						2.0	
		<u>5.70^c</u>	<u>2.20</u>	<u>4.55</u>	5.05	1.5×10^{-6}	0.44	2.3×10^{14}	1.08	0.75 ^c	2.0	
^{242}Am	6.21		2.10	5.00	...						2.0	0.49
		<u>6.40^c</u>	<u>2.30</u>	<u>4.95</u>	...	1.4×10^{-2}	0.38	9×10^{11}	?	0.60 ^c	2.0	0.57
^{243}Am	6.51		2.10	4.85	...						2.0	
		5.75 ^c	2.00	4.90	...	6.5×10^{-6}	0.52	3.3×10^{13}	0.99	0.75 ^c	2.0	
		<u>6.25^c</u>	<u>1.60</u>	<u>4.80</u>	...	1.1×10^{-3}	0.50			0.60 ^c	2.0	0.40
^{244}Am	6.78											
^{245}Am	6.82	5.55 ^c										
^{246}Am	7.31											
^{247}Am	6.53	5.20 ^c										
^{241}Cm	5.06		2.00	4.20	...	1.5×10^{-8}	0.48				2.0	
^{242}Cm	5.36											
^{243}Cm	5.57	5.80 ^c	1.50	4.00	...	3.8×10^{-8}	0.52				2.0	0.50
^{244}Cm	5.85											
^{245}Cm	6.13	6.30 ^f	1.70	4.40	...	2.3×10^{-8}	0.57				2.0	0.30
^{246}Cm	6.81											
^{247}Cm	7.37	6.10 ^f										
^{248}Cm	6.59											
^{249}Cm	6.88	5.50 ^f										
^{250}Cm												

^a B. B. Back, J. P. Bondorf, G. A. Otroschenko, J. Pedersen, and B. Rasmussen, Nucl. Phys. **A165**, 449 (1971).

^b H. C. Britt, S. C. Burnett, and J. D. Cramer, in *Proceedings of the Second International Atomic Energy Agency Symposium on Physics and Chemistry of Fission, Vienna, Austria, 1969* (International Atomic Energy Agency, Vienna, 1969), p. 375.

^c B. B. Back, H. C. Britt, J. D. Garrett, and Ole Hansen, private communication.

^d G. F. Auchampaugh, J. A. Farrell, and D. W. Bergen, Nucl. Phys. **A171**, 31 (1971). Values for E_{II} were reevaluated using the current level-density function in the second well.

^e Assumed value from systematic dependence of other experimental barriers.

^f M. S. Moore and G. A. Keyworth, Phys. Rev. C **3**, 1656 (1971).

The data from $(\alpha, 3n)$ and $(d, 3n)$ reactions to ^{238}Am in its ground-state deformation are the only spallation data available for americium nuclei, and it is seen in Fig. 13 that the "best" parameter set actually gives the poorest fit to these data with predictions that are about a factor of 2 too high. This could indicate some difficulty in the Γ_n/Γ_A calculations but better experimental data are needed before any definite conclusions can be made. [Note added in proof: A recent remeasurement of the $^{237}\text{Np}(\alpha, 3n)^{238}\text{Am}$ cross section (Fleury, Ruddy, Nambodiri, and Alexander^{48a}) gives values considerably less than those reported by Gibson (Ref. 22) and, thus, are in even poorer agreement with the calculations from the "best" parameter set shown in Fig. 13. This comparison may indicate that the current model gives Γ_n/Γ_a values that are systematically too high. Further work on fits to direct reaction fission data (Back, Britt, Garrett, and Hansen^{48b}) also suggest that the current model is overestimating Γ_n/Γ_a by possibly as much as a factor of 2.] The results in Fig. 13 for ^{238}Am illustrate how better spallation data could be used to help determine the heights of the first peak.

3. Curium Nuclei

Measurements are available on fission isomers in only three even-odd curium nuclei and experimental E_A values are not available for all of the necessary nuclei. Therefore, these data were all fitted using calculated E_A values and assuming that $E_B(A+1) = E_B(A)$. The resultant fits are shown in Fig. 16. The experimental spallation data for ^{240}Cm and ^{242}Cm are very uncertain, but the calculations appear to reproduce the correct general magnitude.

B. Values of $\hbar\omega$ from Experimental Half-Lives

The experimental fission-isomer half-lives and spontaneous-fission half-lives for ground-state nuclei can be used to estimate $\hbar\omega_B$ and $\hbar\omega_A$ if three restrictive assumptions are made: (1) Specialization energy effects are not important in odd-particle nuclei; (2) the fission barrier can be adequately described by three smoothly joined parabolic sections; and (3) fission can be adequately treated as a one-dimensional problem. Using these assumptions and the barrier-penetrability code developed by Cramer and Nix,⁴⁹ values of $\hbar\omega_B$ and $\hbar\omega_A$ were estimated from known half-lives and the barrier parameters listed in Table IX. The values obtained are listed in Table IX and the $\hbar\omega_B$ values are plotted in Fig. 17. The estimated errors in the values correspond to the estimated errors in the barrier parameters. For a few cas-

es the $\hbar\omega_A$ values obtained from spontaneous-fission half-lives can be compared to values from the fits to direct-reaction fission experiments; it is seen (Table IX) that for ^{239}Pu and ^{240}Pu the values of $\hbar\omega_A$ from the two sources agree reasonably well but for ^{241}Am and ^{243}Am the spontaneous-fission half-lives imply $\hbar\omega_A$ values significantly larger than those obtained from fits⁴⁸ to the direct reaction data. For ^{242}Am the reported spontaneous-fission half-life of the low-lying 5^- state³⁰ is much too short to be fitted with any reasonable value of $\hbar\omega_A$.

C. Comparison to Other Experimental Data

In a limited number of cases the parameters obtained from fits to the fission-isomer excitation functions can be used to predict other experimental quantities. Of particular interest are the values of $\langle\Gamma_n/\Gamma_f\rangle$, which can be obtained from a comparison of the peak cross section for exciting a particular fission isomer in both $2n$ and $3n$ evaporation reactions, the average level spacing at the neutron binding energy in the two wells (D_I and D_{II}), and estimated values for the cross section for producing fission isomers by (n, γ) reactions.

1. Values of $\langle\Gamma_n/\Gamma_f\rangle$

For isomers in ^{237}Pu , ^{240}Am , ^{242}Am , and ^{244}Am , data are available for population by both $2n$ and $3n$ reactions. In fitting these results the fission-barrier parameters were kept constant; the only additional parameter was $P_f(3n)$, which corresponds to the probability of decay by fission in the initial evaporation for the $3n$ reaction. The values of P_f are related to $\langle\Gamma_n/\Gamma_f\rangle$ averaged over the region of initial excitation energy for the $A+3$ nucleus by

$$P_f = \left\langle \frac{\Gamma_f}{\Gamma_n + \Gamma_f} \right\rangle.$$

Values for $\langle\Gamma_n/\Gamma_f\rangle$ from the experimental P_f values (Table IX) are given in Table X. It is seen that the experimental values agree reasonably well with the calculations from Sec. II B and with the empirical systematics of Vandebosch and Hui-zenga.⁴⁵

2. D_I and D_{II} Level Spacings

From the level-density calculations described in Sec. II B and the E_{II} values in Table IX it is possible to calculate average level spacings in the two wells at the excitation energy corresponding to the neutron binding energy and compare the results to experimental neutron measurements.^{50, 51} Such a comparison is presented in Table XI and

TABLE X. Experimental values of $\langle \Gamma_n / \Gamma_f \rangle$ from comparisons of fits to fission-isomer excitation functions obtained from $2n$ and $3n$ reactions.

Isomeric nucleus	Compound nucleus	Expt. $\langle \Gamma_n / \Gamma_f \rangle$	Calc. Γ_n / Γ_A		Systematics (Ref. 45)
			10 MeV	15 MeV	
^{237}Pu	^{240}Pu	0.54 ± 0.13	0.31	0.18	0.58
^{240}Am	^{243}Am	4 ± 2	2.0	0.9	1.0
^{242}Am	^{245}Am	0.9 ± 0.5	4.8	1.6	2.1
^{244}Am	^{247}Am	1.5 ± 0.6	2.4	0.9	4.6

it is seen that the average calculated level spacings when normalized at ^{240}Pu agree reasonably well for the other nuclei and the ratio $D_{\text{II}}/D_{\text{I}}$ is in good agreement with experimental results. For ^{245}Cm the calculated D_{II} spacing is in reasonable agreement with the intermediate structure that was tentatively identified experimentally⁵¹ but the fitted value of $E_B = 4.4$ MeV for this nucleus would suggest that in this case the intermediate structure should be completely damped out.

Because of the good agreement between calculated and experimental values of $D_{\text{II}}/D_{\text{I}}$ for ^{239}Pu and ^{240}Pu it then appears reasonable to use the current level-density functions in the first and second wells to estimate E_{II} from the measured $D_{\text{II}}/D_{\text{I}}$ ratio for cases where there is no fission-isomer data. In Table XII the results are shown for estimates of E_{II} from experimental $D_{\text{II}}/D_{\text{I}}$ ratios^{51, 52} for ^{239}Pu , ^{241}Pu , ^{243}Pu , and ^{245}Pu . The E_{II} estimates are also listed in Table IX. For ^{243}Pu and ^{245}Pu the E_{II} estimates agree well with the values obtained by Auchampaugh, Farrell, and Bergen⁵² using the level-density expression of Lang and Le Couteur.⁵³

3. Fission Isomers from (n, γ) Reactions

For ^{242}Am and ^{244}Am experimental data are available on the production of fission isomers via (n, γ) reactions⁵⁴ with neutrons in the energy range 0–4

MeV. Using the barriers given in Table IX and the calculated widths $\Gamma_{\gamma}^{\text{II}}$ and Γ_B^{II} the present statistical model can be used to estimate the ratio of isomer to prompt-fission cross sections for (n, γ) reactions. Calculated and experimental isomer to prompt ratios are compared in Table XIII. From this comparison it is seen that at the lowest neutron energies the calculated results are comparable to experimental values but as the neutron energy is increased the calculated values decrease much too rapidly. The sharp decrease in the calculated values may be due partially to the assumption that all γ rays are emitted with an average energy of 1 MeV. A statistical distribution of γ -ray energies would lead to increased values for the isomer to prompt ratios when $E^* \gg E_B$ because the few nuclei which emit high-energy γ rays would be more effectively trapped in the second well. For ^{242}Am and ^{244}Am with the E_B values from Table IX the quantity $E^* - E_B$ is approximately $B_n + 0.5$ MeV.

IV. DISCUSSION

A. Comparison of Experimental and Calculated Barriers

The experimental barrier parameters for isotopes of plutonium, americium, and curium are compared with calculated results in Figs. 18–20,

TABLE XI. Comparison of experimental level spacings with those obtained from the present fits to fission-isomer data.

Nucleus	J	D_{I}		D_{II}		$D_{\text{II}}/D_{\text{I}}$	
		Calc. (eV)	Expt. (eV)	Calc. (keV)	Expt. (keV)	Calc.	Expt.
^{239}Pu	$\frac{1}{2}^+$	8	13^a	0.6 ± 0.3	1^a	77 ± 40	77
^{240}Pu	1^+	3^b	3^a	0.3 ± 0.15	0.46^a	88 ± 40	150
^{241}Pu	$\frac{1}{2}^+$	14	14^a				
^{242}Am	$2^-, 3^-$	0.4	0.56^a				
^{245}Cm	$\frac{1}{2}^+$	10	14^c	1.7 ± 0.8	1^c	173 ± 70	70

^a Reference 50.

^b This value was used to normalize the calculated level spacing to experimental results.

^c Reference 51.

respectively. In these figures the various curves give the results that have been calculated in three independent studies that differ from one another in the type of single-particle potential and shape parametrization used, in the constants of the liquid-drop model, and in the assumed shape dependence of the pairing-interaction strength.

The solid curves give the results that we have calculated in the present study with the diffuse-surface potential of Ref. 8. The constants of the liquid-drop model are taken from the second mass formula of Myers and Swiatecki,⁴¹ and the pairing-interaction strength is kept fixed with deformation. Single-particle specialization energies are neglected. For nuclei with an odd number of neutrons or protons, the odd-particle fluctuations evident in the solid curves arise from variations in the neutron or proton pairing gaps. The ground-state minimum and secondary minimum are determined by varying all three of the symmetric shape coordinates, but the first saddle is restricted to the y family of shapes, and the second (asymmetric) saddle is restricted to shapes described by the fission coordinate y and the mass asymmetry coordinate α_2 .

The dashed curves in Figs. 18 and 20 give the results for even nuclei that Pauli and Ledergerber calculated with a generalized Woods-Saxon potential.⁵⁵ The constants of the liquid-drop model were adjusted to reproduce optimally preliminary values for the experimental heights of the second saddle point.⁵⁶ This leads to a value of 2.84 for the surface asymmetry constant κ in the expression

$$E_s^{(0)} = a_s \left[1 - \kappa \left(\frac{N-Z}{A} \right)^2 \right] A^{2/3}$$

for the surface energy of a spherical nucleus; this is substantially larger than the value of 1.7826 in the Myers-Swiatecki mass formula.⁴¹ The pairing-interaction strength is kept fixed with deformation.

The dot-dashed curves in Figs. 18 and 20 give the results for even nuclei that Möller⁵⁷ has calculated with a modified harmonic-oscillator poten-

tial. The constants of the liquid-drop model are taken from the Myers-Swiatecki mass formula⁴¹; the pairing-interaction strength is assumed proportional to the surface area.

The reduction in energy of the first saddle point by the introduction of axially asymmetric (γ) deformations is taken into account in Figs. 18–20 in an approximate way: The calculated values of E_A for all calculations have been reduced by 0.2 MeV for plutonium isotopes, 0.3 MeV for americium isotopes, and 0.9 MeV for curium isotopes. These reductions are in approximate agreement with the calculations of Larsson, Ragnarsson, and Nilsson.³⁷

The most important conclusion to be drawn from the comparisons in Figs. 18–20 is that the experimental heights of the first and second saddle points and secondary minimum are reproduced in general to within an accuracy of about 1 MeV by the three independent calculations, but that substantial discrepancies remain concerning finer details. In particular, the experimental height of the secondary minimum as a function of increasing neutron number remains roughly constant for plutonium isotopes and decreases somewhat for americium and curium isotopes, whereas the calculated height increases in all cases. Similarly, the experimental height of the second saddle remains roughly constant with increasing neutron number for each series of isotopes, whereas the calculated height increases. In addition, the experimental height of the second saddle decreases with increasing proton number, whereas the calculated height is roughly constant. In a few cases the discrepancies in the calculated and experimental values of E_{II} and E_B are as large as 2 MeV. The calculated and experimental trends in the height of the first peak are in somewhat better agreement, especially for plutonium and curium isotopes. However, in all cases the theoretical values are seen to increase more rapidly with mass number than the experimental results. Other work⁵⁸ indicates that the experimental first peaks of thorium isotopes are somewhat higher than calculated values.

The solid curves are seen to predict a more rap-

TABLE XII. Determination of E_{II} values from experimental D_{II}/D_I measurements.

Nucleus	Expt. D_I (eV)	Expt. D_{II} (keV)	Expt. D_{II}/D_I	E_{II}
²³⁹ Pu $\frac{1}{2}^+$	13 ^a	1 ^a	77	2.20 ± 0.20
²⁴¹ Pu $\frac{1}{2}^+$	14 ^a	0.7 ^a	50	2.00 ± 0.20
²⁴³ Pu $\frac{1}{2}^+$	18.7 ^b	0.6 ^b	32	1.80 ± 0.20
²⁴⁵ Pu $\frac{1}{2}^+$	11.4 ^b	1.5 ^b	132	2.40 ± 0.30

^a Reference 50.

^b Reference 53.

TABLE XIII. Comparison of calculated and experimental (Ref. 54) values for the ratio of isomer to prompt fission cross sections for the reactions $^{241}\text{Am}(n, \gamma)^{242m}\text{Am}$ and $^{243}\text{Am}(n, \gamma)^{244m}\text{Am}$.

E_n	²⁴² Am		²⁴⁴ Am	
	Calculated	Experimental	Calculated	Experimental
0.5	2×10^{-6}		3×10^{-5}	3×10^{-5}
1.5	1×10^{-9}	1.5×10^{-5}	6×10^{-6}	3×10^{-5}
2.5	6×10^{-13}	6×10^{-6}	1×10^{-8}	2×10^{-5}

id variation with neutron number of the heights of the secondary minimum and second saddle point than the dashed and dot-dashed curves. This comparison shows that both the increase in the surface asymmetry constant κ by Pauli and Ledergerber⁵⁵ and the introduction of a surface-dependent pairing strength by Möller⁵⁷ lead to calculated barriers whose variation with neutron number is in better agreement with the experimental results. However, Mosel's recent calculation of fission barriers for nuclei near mass 200, where the saddle-point shapes are highly deformed, indicate that the pairing strength is not proportional to the surface area.⁵⁹ These results taken together suggest that a larger value of κ is required to reproduce the variation with neutron number of experimental fission barriers.

B. Comparison to Results from Previous Model

A comparison of the barrier parameters given in Table IX with those obtained in Ref. 1 using the more simplified statistical model indicates significant differences. In particular the E_{II} values are an average of 0.4 MeV less than estimated previously¹ and the range of deviations is from 0.0 to 0.7 MeV for specific cases. The estimated E_B values are similar to previous values for the plutonium isotopes (except for ²³⁵Pu) but for americium and curium isotopes the estimated E_B values are ~0.6 MeV less than those estimated previously.¹

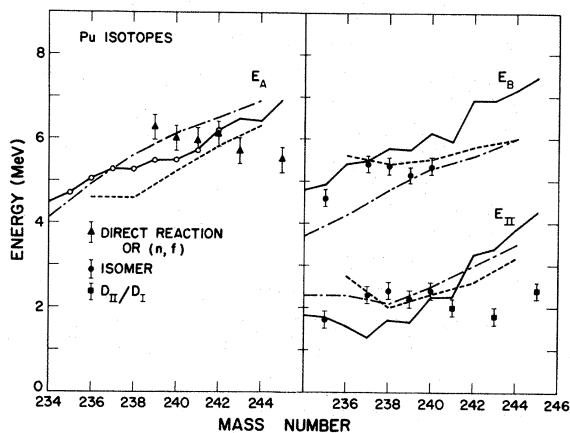


FIG. 18. Experimental values for barrier parameters from Table IX compared to theoretical calculations in the present work (solid line), by Pauli and Ledergerber (Ref. 55) (dashed line), and by Möller (Ref. 57) (dot-dashed line). The open circles indicate cases for which the calculated E_B values were used to calculate ground-state excitation functions shown in Figs. 9 and 12. E_{II} values estimated from D_{II}/D_I spacings are obtained from Ref. 53.

The many differences between the present and previous¹ statistical models make it difficult to quantitatively assess the effects of individual changes on the values deduced for E_{II} and E_B from fits to experimental isomer excitation functions. However, the major differences between the two models can be grouped into two general categories: (1) differences in the shapes of the level-density functions and (2) different values used for some of the fixed parameters in the model (e.g. E_A values) or different assumptions used for the systematic variation of the parameters (e.g. systematic odd-even fluctuations for americium barriers).

The level-density functions are different in two important ways from those used in the previous model. First, because of the differences in shell and pairing energies the level-density functions have different shapes at each minimum and maximum in the potential-energy surface whereas with the generalized Gilbert and Cameron level densities used previously¹ the level-density functions all had the same general shape except that a larger level-density parameter a was used at the two maxima. The results of this change are that the detailed shapes of the calculated excitation functions are dependent on the specific parameter values and the odd or even character of the nuclei involved to a much larger extent than was true with the previous model or with models which employ a constant-temperature level density⁶⁰ (e.g. see Figs. 13–15). These differences in shapes for the calculated excitation functions tend to give slightly better fits to the experimental data and are the primary cause of the fluctuations in the differences

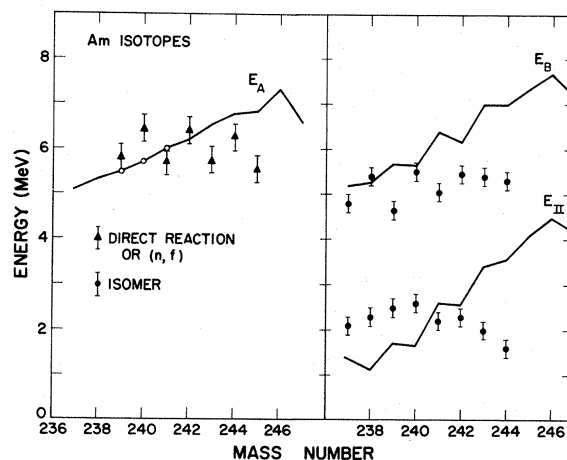


FIG. 19. Experimental values for barrier parameters from Table IX compared to theoretical calculations in the present work. The open circles indicate cases for which the calculated E_A values were used to calculate ground-state excitation functions shown in Fig. 13.

between the current barrier parameters and those deduced previously.¹

The second major difference in the level densities is that the current model uses the single-particle levels at the second *asymmetric* saddle, which corresponds to a large negative shell energy. In the previous model it was assumed that the level density at the second saddle had the same form as at the first saddle, which was equivalent to assuming a positive shell energy at this point. In the previous model the values used for a_f for americium and curium isotopes were significantly larger than for plutonium isotopes; this accounts for the systematic difference when E_B values from the two analyses are compared.

The other major difference between the present fits and the previous ones¹ is that a different set of E_A values is used, and for the americium isotopes the data are fitted allowing for odd-even fluctuations in E_A and E_B . As is shown in Table IX, for the americium isotopes different sets of E_A values and allowing odd-even effects can give differences of up to 0.4 MeV in the fitted values of E_{II} and E_B .

C. Anomalies in Americium Barriers

In the results shown in Figs. 18 and 19 it is seen that the experimental barrier parameters for plutonium isotopes are approximately independent of mass number but for americium isotopes the values of E_A and E_B for odd-odd nuclei are 0.5–1.0 MeV greater than for neighboring odd-proton-

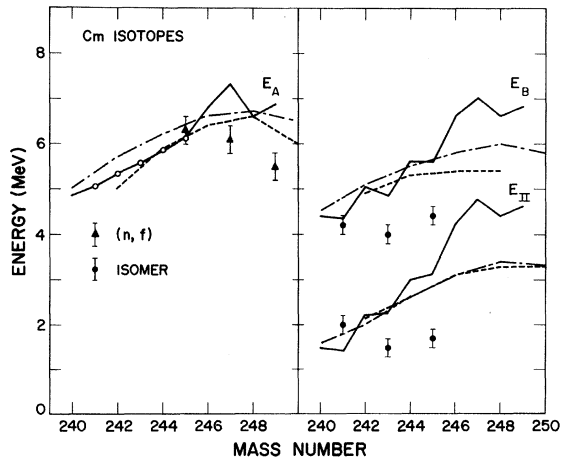


FIG. 20. Experimental values for barrier parameters from Table IX compared to theoretical calculations in the present work (solid line), by Pauli and Ledergerber (Ref. 55) (dashed line), and by Möller (Ref. 57) (dot-dashed line). The open circles indicate cases for which the calculated E_A values were used to calculate ground-state excitation functions in Fig. 16.

even-neutron nuclei. Figure 17 shows that the constant barrier heights and odd-even fluctuations in isomer half-lives for the plutonium isotopes lead to odd-even fluctuations in the values deduced for $\hbar\omega_B$. However, for the americium isotopes the odd-even fluctuations in E_B are large enough to account for the odd-even isomer half-life fluctuations so that the deduced values for $\hbar\omega_B$ do not show any significant structure. In contrast the values for E_{II} for the americium isotopes do not seem to show systematic odd-even fluctuations.

These odd-even fluctuations which occur in americium but not plutonium isotopes and which are present at the saddle points but apparently not at the secondary minimum are very puzzling and cannot be understood with any of our present ideas about fission barriers. It is possible that part of this effect could be due to deficiencies in the models used to extract barriers from the experimental results, but it appears unlikely that the entire effect can be accounted for in this manner. The values of E_B from fits to the isomer excitation functions are ~ 0.5 – 1.0 MeV less than those estimated with the previous empirical model¹ but the odd-even fluctuations in E_B remain about the same in both cases. In the isomer fits the value of E_B is most sensitive to the peak isomer/prompt ratio and about the only way an artificial odd-even fluctuation could arise in the deduced E_B values would be if a large fraction of the isomeric cross section was systematically not observed for the odd-mass americium isotopes. Such a situation could occur if the isomeric state decayed primarily by γ rays or by a short half-life fission branch that has not yet been observed. Either of these two possibilities seems unlikely. For the models^{47, 48} used to obtain E_A values from direct reaction data there is a correlation between the fitted values of E_A and $\hbar\omega_A$ in the analysis for even-even nuclei but it appears unlikely that the published values⁴⁷ will change by more than about 0.3 MeV. For odd- A and odd-odd nuclei E_A and $\hbar\omega_A$ values were determined from fits to experimental data using a simplified statistical model⁴⁸ which assumed smooth level densities and widths from the same calculations described in Sec. II B and assumed that there was complete damping of the fission degree of freedom into the compound states in the second well. For the americium isotopes E_A – E_B is large enough so that the fission probability distributions are sensitive only to E_A and $\hbar\omega_A$ and both parameters can be determined uniquely from the experimental data. Major deficiencies in this statistical model are that the level-density calculations seriously underestimate the density of levels at low excitation energies (<1 MeV) for even-even and odd- A nuclei and the model does not al-

low for the gross differences at low energy in the distribution of states of different spin and parity. These effects are currently being investigated and preliminary results⁴⁸ indicate that a more realistic model may give a reduced odd-even fluctuation in the E_A values. At present it appears that these deficiencies in the model may account for one half of the apparent odd-even fluctuation shown in Table IX and most likely the changes from the values given in Table IX will be less than ~ 0.3 MeV.

One possible source of odd-even fluctuations could be from differences in the pairing gaps at the maxima and minima of the potential energy surface but this explanation seems unlikely for two reasons. First, any differences should be similar for plutonium and americium isotopes. Secondly, the first and second saddle points correspond to large positive and large negative shell corrections, respectively, and consequently one would not expect correlated fluctuations in the heights of the two barriers due to pairing effects alone.

Alternatively, the observed odd-even fluctuations might result from the odd-odd americium isotopes following a path to fission that is slightly different from the path followed by odd-even isotopes. Such an effect might arise if the addition of an odd neutron significantly changed either the character of the potential energy surface or possibly modified the inertias in a nonlinear way. A realistic estimate of the possibility of such an effect awaits more detailed calculations of the dynamics of the fission process.

V. SUMMARY AND CONCLUSION

In an attempt to obtain more accurate experimental information on the fission barriers of actinide nuclei, we have reanalyzed fission-isomer data by means of a statistical model that contains a realistic calculation of compound-nuclear level densities. In particular, the level densities are obtained microscopically in terms of single-particle states calculated at the first minimum, first saddle point, second minimum, and second saddle point in the fission barrier; the effects of nuclear pairing are included. In this way the dependence of the level density upon both deformation and energy is taken into account automatically.

This analysis yielded improved values for the heights of the second minimum and second saddle points in several isotopes of plutonium, americium, and curium. These values, which are accu-

rate to within about 0.2 MeV, are in most cases smaller than previous values¹ by varying amounts from 0–1 MeV. Values for the height of the first saddle were obtained from fission cross-section measurements. Once these heights were established, the experimental fission-isomer half-life and half-life for spontaneous fission from the ground state were used to determine the effective widths of the two peaks in the barrier (expressed in terms of values for $\hbar\omega_A$ and $\hbar\omega_B$).

The experimental heights of the first and second saddle points and secondary minimum were compared with three independent calculations that were performed within the macroscopic-microscopic method. The experimental heights are reproduced in general to within an accuracy of about 1 MeV by the calculations, but some serious discrepancies remain concerning finer details, including errors as large as 2 MeV in a few cases. The variation of the barrier heights with neutron number is reproduced better with the Pauli-Lederger value of 2.84 for the surface asymmetry constant than with the Myers-Swiatecki value of 1.7826.

The differences encountered here between calculated and experimental barrier heights are approximately the same magnitude as the differences between calculated and experimental ground-state masses of nuclei throughout the Periodic Table, where the rms deviation is about 0.7 MeV, but where appreciable systematic errors remain, including errors as large as about 2 MeV for several nuclei.⁶¹ These results taken together imply that at present the nominal accuracy of the macroscopic-microscopic method is about 1 MeV, but that errors of about 2 MeV can be expected in some cases.

ACKNOWLEDGMENTS

We are very grateful to K. L. Wolf and J. P. Unik for measuring the $^{236}\text{U}(\alpha, 3n)^{237\text{m}}\text{Pu}$ excitation function which was used to test the calculations. We would also like to thank them and G. Sletten and P. Limkilde for communicating their results to us before publication. We would like to thank C. F. Tsang for sending results of his calculations for comparison with our single-particle spectra. We are pleased to acknowledge useful discussions with B. B. Back, S. Björnholm, J. D. Garrett, Ole Hansen, J. E. Lynn, and R. Vandebosch. We would like to thank M. Blann for supplying the pre-equilibrium neutron emission calculations that were used in the statistical model calculations.

*Work performed under the auspices of the U. S. Atomic Energy Commission.

¹H. C. Britt, S. C. Burnett, B. H. Erkkila, J. E. Lynn, and W. E. Stein, *Phys. Rev. C* **4**, 1444 (1971).

²A. Gilbert and A. G. W. Cameron, *Can. J. Phys.* **43**, 1446 (1965).

³V. S. Ramamurthy, S. S. Kapoor, and S. K. Kataria, *Phys. Rev. Letters* **25**, 386 (1970).

⁴L. G. Moretto and R. Stella, *Phys. Letters* **32B**, 558 (1970); L. G. Moretto, *Phys. Letters* **34B**, 191 (1971); L. G. Moretto, *Nucl. Phys.* **A180**, 337 (1972).

⁵F. C. Williams, Jr., G. Chan, and J. R. Huizenga, *Nucl. Phys.* **A187**, 225 (1972).

⁶P. Decowski, W. Grochulski, A. Marcinkowski, K. Siwek, and Z. Wilhelmi, *Nucl. Phys.* **A110**, 129 (1968).

⁷V. M. Strutinsky, *Nucl. Phys.* **A95**, 420 (1967); **A122**, 1 (1968); S. Bjørnholm and V. M. Strutinsky, *ibid.* **A136**, 1 (1969).

⁸M. Bolsterli, E. O. Fiset, J. R. Nix, and J. L. Norton, *Phys. Rev. C* **5**, 1050 (1972).

⁹K. L. Wolf and J. P. Unik, private communication.

¹⁰G. Sletten and P. Limkilde, private communication.

¹¹S. M. Polikanov and G. Sletten, *Nucl. Phys.* **A151**, 656 (1970).

¹²G. Sletten, private communication.

¹³H. C. Britt, B. H. Erkkila, and B. B. Back, *Phys. Rev. C* **6**, 1090 (1972).

¹⁴N. L. Lark, G. Sletten, J. Pedersen, and S. Bjørnholm, *Nucl. Phys.* **A139**, 481 (1969).

¹⁵S. Bjørnholm, J. Borggreen, L. Westgaard, and V. A. Karnaukhov, *Nucl. Phys.* **A95**, 513 (1967).

¹⁶G. N. Flerov, A. A. Pleve, S. M. Polikanov, S. P. Tretyakova, N. Martalogu, D. Poenaru, M. Sezon, I. Vîlcov, and N. Vîlcov, *Nucl. Phys.* **A97**, 444 (1967).

¹⁷K. L. Wolf and J. P. Unik, private communication; *Phys. Letters* **38B**, 405 (1972).

¹⁸R. Vandenbosch, T. D. Thomas, S. E. Vandenbosch, R. A. Glass, and G. T. Seaborg, *Phys. Rev.* **111**, 1358 (1958).

¹⁹G. R. Bethune, H. C. Britt, and B. H. Erkkila, *Phys. Rev. C* **6**, 1087 (1972).

²⁰J. A. Coleman, University of California, Lawrence Radiation Laboratory Report No. UCRL-8186, 1958 (unpublished).

²¹J. Wing, W. J. Rampler, A. L. Harkness, and J. R. Huizenga, *Phys. Rev.* **114**, 163 (1959).

²²W. M. Gibson, University of California, Lawrence Radiation Laboratory Report No. UCRL-3493, 1956 (unpublished).

²³R. A. Glass, R. J. Carr, J. W. Cobble, and G. T. Seaborg, *Phys. Rev.* **104**, 434 (1956).

²⁴J. K. Temperley, J. A. Morrissey, and S. L. Bacharach, *Nucl. Phys.* **A175**, 433 (1971); P. A. Russo, R. Vandenbosch, M. Metha, J. R. Tesmer, and K. L. Wolf, *Phys. Rev. C* **3**, 1595 (1971).

²⁵S. M. Polikanov, V. A. Druin, V. A. Karnaukhov, V. L. Mikheev, A. A. Pleve, N. K. Skobelev, V. G. Subbotin, G. M. Ter-Akopjan, and V. A. Fomichev, *Zh. Eksperim. i Teor. Fiz.* **42**, 1464 (1962) [transl.: *Soviet Phys. - JETP* **15**, 1016 (1962)].

²⁶S. Bjørnholm, J. Borggreen, Yu. P. Gangrsky, and G. Sletten, *Yadern. Fiz.* **8**, 459 (1968) [transl.: *Soviet J. Nucl. Phys.* **8**, 267 (1969)].

²⁷V. A. Druin *et al.*, *Zh. Eksperim. i Teor. Fiz.* **40**,

1296 (1961) [transl.: *Soviet Phys. - JETP* **13**, 913 (1961)].

²⁸E. Segrè, *Phys. Rev.* **86**, 21 (1952).

²⁹L. Z. Malkin *et al.*, *At. Energ. (USSR)* **15**, 158 (1963) [transl.: *Soviet J. At. Energy* **15**, 851 (1964)].

³⁰J. T. Caldwell, S. C. Fultz, C. D. Bowman, and R. W. Hoff, *Phys. Rev.* **155**, 1309 (1967).

³¹B. M. Aleksandrov, L. S. Krivokhatsky, L. Z. Malkin, and K. A. Petrzhak, *At. Energ. (USSR)* **20**, 315 (1966) [transl.: *Soviet J. At. Energy* **20**, 352 (1966)].

³²M. Blann, *Phys. Rev. Letters* **28**, 757 (1972); M. Blann, private communication.

³³S. Jägare, *Nucl. Phys.* **A137**, 241 (1969); *Phys. Letters* **32B**, 571 (1970).

³⁴M. Brack, J. Damgaard, A. S. Jensen, H. C. Pauli, V. M. Strutinsky, and C. Y. Wong, *Rev. Mod. Phys.* **44**, 320 (1972).

³⁵P. Möller and S. G. Nilsson, *Phys. Letters* **31B**, 283 (1970).

³⁶J. R. Nix, *Ann. Rev. Nucl. Sci.* (to be published).

³⁷S. E. Larsson, I. Ragnarsson, and S. G. Nilsson, *Phys. Letters* **38B**, 269 (1972).

³⁸U. Götz, H. C. Pauli, and K. Junker, *Phys. Letters* **39B**, 436 (1972).

³⁹E. Wigner, *Trans. Faraday Soc.* **34**, 29 (1938).

⁴⁰N. Bohr and J. A. Wheeler, *Phys. Rev.* **56**, 426 (1939).

⁴¹W. D. Myers and W. J. Swiatecki, *Arkiv Fysik* **36**, 343 (1967).

⁴²W. D. Myers, *Nucl. Phys.* **A145**, 387 (1970).

⁴³J. R. Nix, *Nucl. Phys.* **A130**, 241 (1969).

⁴⁴A. Bohr and B. R. Mottelson, *Nuclear Structure* (Benjamin, New York, 1969), Vol. I, p. 281 ff.

⁴⁵R. Vandenbosch and J. R. Huizenga, in *Proceedings of the Second United Nations International Conference on the Peaceful Uses of Atomic Energy, Geneva, 1958* (United Nations, Geneva, 1958), Vol. 15, p. 284.

⁴⁶C. F. Tsang, private communication; S. G. Nilsson, C. F. Tsang, A. Sobiczewski, Z. Szymanski, S. Wycech, C. Gustafsson, I. L. Lamm, P. Möller, and B. Nilsson, *Nucl. Phys.* **A131**, 1 (1969).

⁴⁷B. B. Back, J. P. Bondorf, G. A. Otroschenko, J. Pedersen, and B. Rasmussen, *Nucl. Phys.* **A165**, 449 (1971).

⁴⁸B. B. Back, H. C. Britt, J. D. Garrett, and O. Hansen, private communication.

^{48a}A. Fleury, F. H. Ruddy, M. N. Namboodiri, and J. M. Alexander, to be published.

^{48b}B. B. Back, H. C. Britt, J. D. Garrett, and O. Hansen, private communication.

⁴⁹J. D. Cramer and J. R. Nix, *Phys. Rev. C* **2**, 1048 (1970).

⁵⁰J. E. Lynn, in *Proceedings of the Second International Atomic Energy Agency Symposium on Physics and Chemistry of Fission, Vienna, 1969* (International Atomic Energy Agency, Vienna, 1969), p. 249.

⁵¹M. S. Moore and G. A. Keyworth, *Phys. Rev. C* **3**, 1656 (1971).

⁵²G. F. Auchampaugh, J. A. Farrell, and D. W. Bergen, *Nucl. Phys.* **A171**, 31 (1971).

⁵³J. M. B. Lang and K. J. Le Couteur, *Proc. Phys. Soc.* **A67**, 586 (1954).

⁵⁴I. Boca, N. Martalogu, M. Sezon, I. Vîlcov, N. Vîlcov, G. N. Flerov, A. A. Pleve, S. M. Polikanov, and S. P. Tretyakova, *Nucl. Phys.* **A134**, 541 (1969).

⁵⁵H. C. Pauli and T. Ledergerber, *Nucl. Phys.* **A175**, 545 (1971).

⁵⁶S. Bjørnholm and J. E. Lynn, unpublished preliminary results.

⁵⁷P. Möller, Nucl. Phys. (to be published).

⁵⁸B. B. Back, H. C. Britt, J. D. Garrett, and O. Hansen, Phys. Rev. Letters 28, 1707 (1972).

⁵⁹U. Mosel, Phys. Rev. C 6, 971 (1972).

⁶⁰R. Vandenbosch, Phys. Rev. C 5, 1428 (1972).

⁶¹P. A. Seeger, in Proceedings of the Fourth International Conference on Atomic Masses and Fundamental Constants, Teddington, England, 1971 (to be published).

PHYSICAL REVIEW C

VOLUME 7, NUMBER 2

FEBRUARY 1973

Neutron Resonance Spectroscopy. XI. The Separated Isotopes of Yb[†]

H. I. Liou, H. S. Camarda,* G. Hacken, F. Rahn, J. Rainwater, M. Slagowitz, and S. Wynchank‡

Columbia University, New York, New York 10027

(Received 26 July 1972)

Neutron time-of-flight resonance spectroscopy results, using the Nevis synchrocyclotron, for the separated Yb isotopes (170, 171, 172, 173, 174, 176) are given. Transmission and self-indication measurements were made for several sample thicknesses of each isotope. Resonance parameters, Γ_n^0 (or $g\Gamma_n^0$), are given to ~ 1.8 keV for 171 and 173, and to ~ 10 keV for 172, 174, and 176. Levels in 170 were those seen in the natural element, but not in the 171–176 isotopes. Many resonance Γ_γ and J values were also obtained for 171 and 173, and a few Γ_γ values for 172 and 174. The $10^4 S_0$ values are 2.25 ± 1.0 , 1.86 ± 0.16 , 1.68 ± 0.20 , 1.60 ± 0.28 , 1.62 ± 0.21 , and 2.29 ± 0.32 for 170, 171, 172, 173, 174, and 176, respectively. $\langle \Gamma_\gamma \rangle = 76.5$ meV (37 levels), 72.3 meV (3 levels), and 73.8 meV (33 levels) for 171, 172, and 173, respectively. A shape fit to the asymmetric level in 174 at 342.7 eV gave $R' = (7.9 \pm 0.5)$ fm. The increasing σ below ~ 100 eV for 174 and natural Yb, and the known thermal 174 partial cross sections, were fitted assuming a bound 174 level at $E_0 = -25$ eV, $\Gamma_n^0 = 160$ meV. Comparison of the $(g\Gamma_n^0)^{1/2}$ distributions with Porter-Thomas theory and the nearest-neighbor energy spacings with the Wigner theory gave best agreement for 172, as did other statistical orthogonal ensemble (O.E.) tests. There were missing weak s levels for 171 and 173 and extra p levels for 176. The 174 and 176 results were also compatible with O.E. theory but provided poorer test cases than 172.

I. INTRODUCTION

This is the eleventh in a series of papers¹ reporting results of high-resolution neutron resonance time-of-flight spectroscopy using the Columbia University Nevis synchrocyclotron as a source. The paper presents resonance parameter results for the separated isotopes of Yb over the energy range to 1.7 or 1.8 keV for the odd isotopes ¹⁷¹Yb and ¹⁷³Yb, and to 10 or 20 keV for the even isotopes ¹⁷²Yb, ¹⁷⁴Yb, and ¹⁷⁶Yb. In addition, we have measurements using natural Yb samples which permit us to evaluate level parameters for a number of levels of ¹⁷⁰Yb (3.03 at.% in natural Yb) to ~ 1300 eV which are not hidden by levels in the more abundant isotopes. Our study of the Yb isotopes has extended over a number of years. The analysis of earlier Yb data obtained was given in the Columbia University Ph.D. thesis of Liou. Since the measurements obtained later were of such superior quality to our earlier measurements, publication was delayed to permit a thorough analysis of the data which form the main basis for this paper. Liou has been mainly responsible for this data analysis, while all of the authors were involved in

carrying through the later measurements.

We have previously reported results (VIII) for some of the other data obtained during these measurements, along with a description of the experimental details and data analysis techniques. The Er results, especially for ¹⁶⁶Er, gave the first conclusive evidence supporting the statistical orthogonal ensemble (O.E.) theory for the systematics of level spacings for single s populations. This was supported by the results (IX) for ¹⁵²Sm and some other favorable nuclei² in the mass range $150 \leq A \leq 190$. The agreement with the theory is also excellent for ¹⁷²Yb which is discussed in this paper. The most favorable nuclei for such tests (in this mass interval) seem to be the lowest-mass even-even isotopes having relatively high abundance in the natural elements. It is a mass region where there is a peak in the s strength function, S_0 , and the p strength function S_1 is appreciably smaller. The effect favoring the lightest even-even isotope for a given element presumably relates to a trend for S_0 to decrease as neutrons are added for a given Z , coupled with a corresponding increase in S_1 . These effects have been mentioned by others.³ While this trend for Yb seems to be generally fol-